

UNIVERSIDADE ESTADUAL DE CAMPINAS
SISTEMA DE BIBLIOTECAS DA UNICAMP
REPOSITÓRIO DA PRODUÇÃO CIENTÍFICA E INTELLECTUAL DA UNICAMP

Versão do arquivo anexado / Version of attached file:

Versão do Editor / Published Version

Mais informações no site da editora / Further information on publisher's website:

<https://www.nature.com/articles/s41558-023-01776-4>

DOI: <https://doi.org/10.1038/s41558-023-01776-4>

Direitos autorais / Publisher's copyright statement:

©2023 by Nature. All rights reserved.

DIRETORIA DE TRATAMENTO DA INFORMAÇÃO

Cidade Universitária Zeferino Vaz Barão Geraldo

CEP 13083-970 – Campinas SP

Fone: (19) 3521-6493

<http://www.repositorio.unicamp.br>

Sensitivity of South American tropical forests to an extreme climate anomaly

Received: 2 December 2021

Accepted: 21 July 2023

Published online: 4 September 2023

 Check for updates

A list of authors and their affiliations appears at the end of the paper

The tropical forest carbon sink is known to be drought sensitive, but it is unclear which forests are the most vulnerable to extreme events. Forests with hotter and drier baseline conditions may be protected by prior adaptation, or more vulnerable because they operate closer to physiological limits. Here we report that forests in drier South American climates experienced the greatest impacts of the 2015–2016 El Niño, indicating greater vulnerability to extreme temperatures and drought. The long-term, ground-measured tree-by-tree responses of 123 forest plots across tropical South America show that the biomass carbon sink ceased during the event with carbon balance becoming indistinguishable from zero ($-0.02 \pm 0.37 \text{ Mg C ha}^{-1}$ per year). However, intact tropical South American forests overall were no more sensitive to the extreme 2015–2016 El Niño than to previous less intense events, remaining a key defence against climate change as long as they are protected.

Intact tropical forests are a key component of the Earth system, storing and sequestering large amounts of carbon¹. Climate-driven changes to the capacity of tropical forests to sequester and store carbon as biomass could thus have important consequences for the evolution of climate change itself. Among the key processes governing the carbon balance of tropical ecosystems are the rates of tree growth, which takes carbon into the biomass pool, and tree mortality, which transfers it to necromass. In turn, both growth and mortality are likely to depend closely on plant available water, temperature and their fluctuations. How sensitive tropical forests are to atmospheric warming and drying remains poorly constrained and one of the major sources of uncertainty in vegetation models and coupled climate–carbon cycle models^{2–4}. Understanding ecosystem–climate relationships is particularly critical in South America, which still harbours the most extensive and diverse tropical forests in the world^{5,6}.

Measurements from long-term inventory plots suggest that Amazonian forests have contributed a major carbon sink for decades but that this carbon sink has been declining since the early 1990s (ref. 7), and may cease before 2040 (ref. 8). These tree-by-tree measurements also suggest that the tropical biomass carbon sink is vulnerable to short-term warming^{8,9} and drought, with ground data showing temporary suspension of the sink following both the 2005 (ref. 10) and 2010 (ref. 11) Amazon droughts. Meanwhile, relatively little is known about South American forest carbon dynamics and drought sensitivity beyond Amazonia, although the future of all these forests and their capacity to mitigate climate change also depends on

how they will function under changed conditions. Recent work suggests the long-term risk of losing the carbon sink extends to some seasonal Atlantic forests¹² and that Southeast Amazon forests may have already switched from functioning as a carbon sink to a carbon source¹³. While the dominant source in the Southeast Amazon is likely to be degraded forests^{13–15}, we lack an integrated analysis of the responses of aboveground biomass dynamics to extreme climate anomalies here, let alone across South American tropical forests using ground records¹⁶. In principle, hotter and drier forests may be either more resistant to hotter and drier climates, protected by evolutionary adaptation to extreme conditions, or more vulnerable due to operating closer to physiological thresholds^{17,18}.

The 2015–2016 El Niño event caused record heat and drought across South America¹⁹ and presented a unique opportunity to evaluate both the impact of long-term climate baselines and short-term climate anomalies on South American forests. In this Article, we assessed the impact of the 2015–2016 El Niño on South American tropical forests using 123 long-term monitoring plots in the RAINFOR and PPBio networks, the largest on-the-ground dataset yet mobilized to address the impact of a single tropical drought. These structurally intact forest plots span Amazonian and Atlantic forests including those that are transitional with dry forests and Cerrado. We investigate the impact of the 2015–2016 El Niño heat and drought on the temporal patterns of net aboveground carbon biomass (net carbon), on carbon gains from recruitment and productivity, and on biomass mortality (carbon losses). We normalize net carbon, gains and losses

✉ e-mail: acrbennett@gmail.com

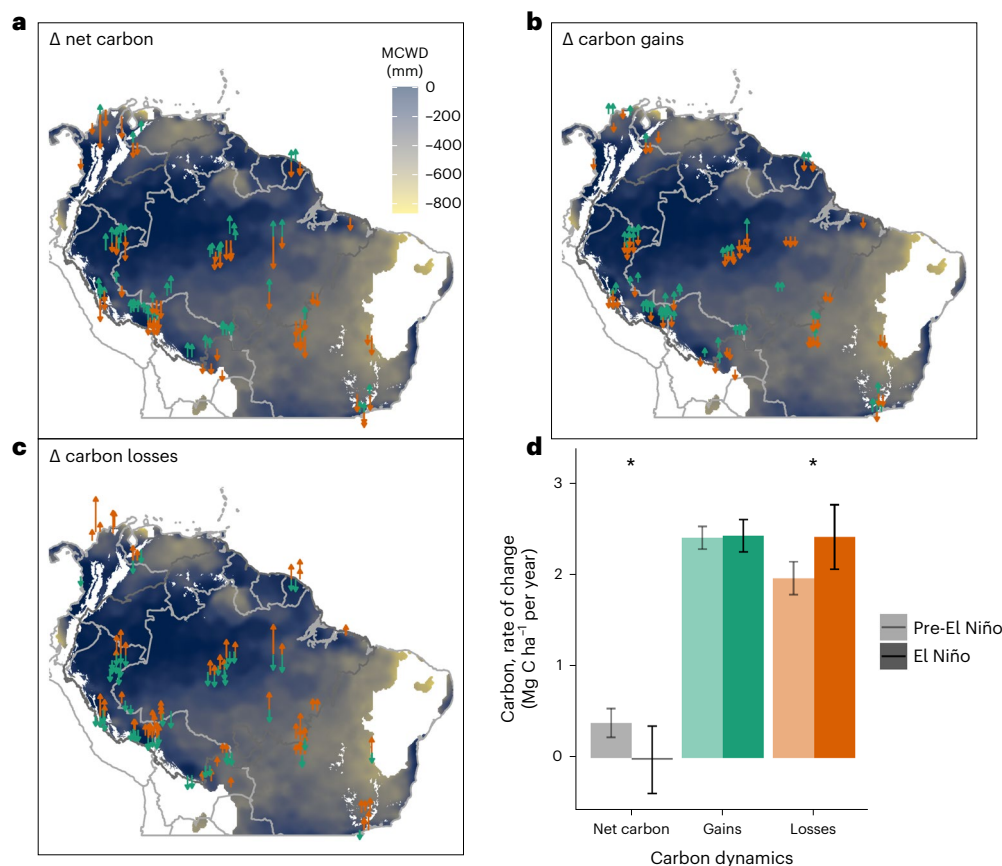


Fig. 1 | Aboveground carbon changes in 123 neotropical forest plots during the 2015–2016 El Niño event. a–d, Maps (a–c) with arrows representing the magnitude and direction of measured change and approximate location of each plot and biomass carbon dynamics (d) pre- and during the 2015–2016 El Niño event. For a–c, orange arrows indicate negative effects on biomass stocks (for example, decreasing net change, increasing losses) and green arrows indicate positive effects on biomass stocks (for example, increasing gains). El Niño – pre-El Niño aboveground net carbon, Δ net carbon (a). El Niño – pre-

El Niño aboveground carbon gains, Δ carbon gains (b). El Niño – pre-El Niño aboveground carbon losses, Δ carbon losses (c). The background shading shows pre-El Niño MCWD (mean MCWD for May 2005 to April 2015) across the climate space, not the current extent of tropical forests. For d, $n = 123$ plots, error bars represent 95% CIs, centred on the mean, and “*” indicates significant paired, two-sided t -test, net carbon $P = 0.049$, losses $P = 0.017$. The full scatter of the data can be seen in Extended Data Fig. 3.

to a percentage change with respect to the pre-El Niño baseline so that we can compare forests with a range of initial size and dynamics. We analyse instantaneous stem mortality rates, size classes and mean wood density of the dying trees to understand which trees are dying. Finally, we assess whether the impacts of the extreme climate event on tropical forests interact with the long-term baseline climate, to help understand if specific regions are pre-adapted for resistance to extreme events or conversely are highly susceptible to losing biomass carbon.

Almost all plots warmed during the 2015–2016 El Niño. Comparing census intervals that capture the event (mean September 2014 to May 2017) with the pre-El Niño census period (mean May 2001 to September 2014), 119 of 123 plots had higher mean monthly temperatures, by an average of $+0.53 \pm 0.10$ °C (paired t -test, $P < 0.0001$, maps of pre-El Niño climate anomalies are included in Extended Data Fig. 1). Plots also had greater water deficits during the El Niño census interval than in their pre-El Niño monitoring period, with 99 having more negative maximum cumulative water deficit (MCWD) (mean difference -66 ± 25 mm, paired t -test, $P < 0.0001$), and 96 having lower annual precipitation (mean difference -215 ± 100 mm per year, paired t -test, $P < 0.0001$). Where it was anomalously hotter it was also anomalously drier—the anomalies of temperature and MCWD were significantly positively correlated over the census interval that captures the El Niño (linear model $P = 0.008$, Extended Data Fig. 2).

The long-term pre-El Niño (mean 2001.4 to 2014.7) biomass carbon sink, 0.38 ± 0.16 Mg C ha⁻¹ per year, declined significantly during the El Niño census interval (mean 2014.7 to 2017.4) to become indistinguishable from zero, -0.02 ± 0.37 Mg C ha⁻¹ per year, (paired t -test, $n = 123$, $P = 0.0495$, Fig. 1d). The net change in carbon is driven by a significant increase in carbon losses due to biomass mortality (from 1.96 to 2.41 Mg C ha⁻¹ per year, $P = 0.02$), while there was no change in carbon gains from tree growth and new tree recruitment (2.40 Mg C ha⁻¹ per year pre-El Niño and 2.43 Mg C ha⁻¹ per year during the El Niño, $P = 0.7$). Hence, during the high temperatures and drought of the 2015–2016 El Niño, the 123 forest plots were not a significant biomass carbon sink and this contrasted with their long-term pre-El Niño behaviour. We note that the extreme climate anomaly was shorter than the 2.7 year monitoring window, so given the pre-El Niño sink these forests are likely to have lost biomass carbon on average during and after the event itself.

Higher temperature anomalies significantly increased relative carbon losses from tree mortality (linear model $P = 0.02$, Fig. 2e). The increased losses result in a significant effect of temperature anomalies on net biomass carbon anomalies (linear model $P = 0.02$, Fig. 2a). Thus, relative to the pre-El Niño baseline of increasing biomass, forests subjected to a 0.5 °C increase in temperature lost 0.5% of aboveground biomass carbon (Fig. 2a).

Stronger drought anomalies increased relative carbon losses (linear model, $P = 0.07$, two-tailed Kendall's τ $P = 0.01$, Fig. 2f) and

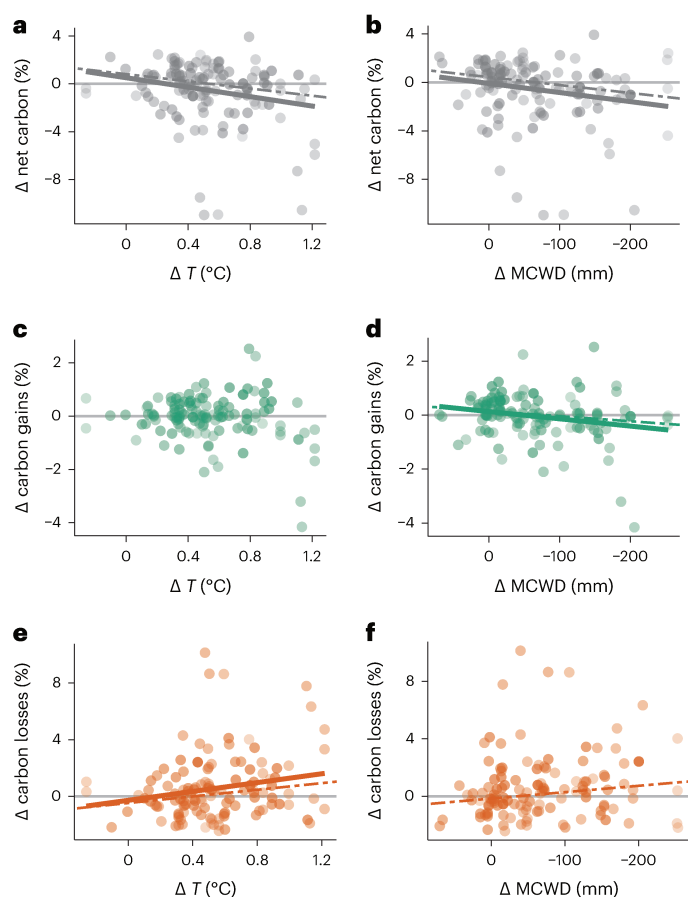


Fig. 2 | Effects of the 2015–2016 El Niño climate anomaly on aboveground biomass carbon dynamics in 123 neotropical forest plots. a–f. Temperature anomaly (a, c and e) and drought anomaly (b, d and f) impacts on aboveground biomass carbon, with forest response variables expressed as relative change. Carbon changes are computed relative to pre-El Niño aboveground biomass carbon for each plot, for example (El Niño carbon gains – pre-El Niño carbon gains)/pre-El Niño aboveground biomass carbon. The net carbon change (a and b), carbon gains from recruitment and growth (c and d) and carbon losses from mortality (e and f) are shown for 123 long-term inventory plots. The intensity of temperature change, ΔT (°C) (a, c and e) is mean monthly temperature in El Niño minus mean monthly temperature pre-El Niño, using the census dates of the plot censuses. The intensity of the change in dry season strength is calculated as $\Delta MCWD$ (b, d and f), which is the difference between maximum MCWD in El Niño and mean MCWD in pre-El Niño. Point shading from light to dark denotes greater weighting, with plots and line of best fit weighted by an empirically derived combination of pre-El Niño plot monitoring length and plot area for each response variable. Solid lines represent significant linear models ($P < 0.05$) and dashed lines represent significant one-tailed Kendall's τ correlation tests using rank-based linear model estimation ($P < 0.05$). Slopes, intercepts and P values for significant linear models are as follows: A: $y = -2x + 0.5$, $P = 0.01$, B: $y = -0.008x - 0.08$, $P = 0.02$, D: $y = -0.003x + 0.1$, $P = 0.01$, E: $y = 1.6x - 0.3$, $P = 0.02$, F: linear model is not significant, $P = 0.07$, but rank-based model is, $P = 0.01$. See Extended Data Fig. 4 for an alternative analysis excluding censuses before 2000, and Extended Data Fig. 5 for an alternative analysis with carbon changes in absolute terms.

significantly reduced carbon gains (linear model $P = 0.01$, Fig. 2d). Thus, stronger drought anomalies significantly reduced aboveground biomass carbon (linear model $P = 0.02$, Fig. 2b). Relative to the pre-El Niño baseline, forests subjected to a 100 mm stronger MCWD lost 0.8% of aboveground biomass carbon (Fig. 2b). These trends are not driven by wetter plots benefitting during the El Niño, relationships being similar when the 22 plots that were slightly wetter during their El Niño census interval are excluded.

Forests with drier long-term climate lost more biomass carbon in the 2015–2016 El Niño than wetter forests (Fig. 3). Thus, plots with stronger pre-El Niño water deficits lost more aboveground biomass carbon through mortality (linear model $P = 0.02$, Fig. 3f) and had greater reductions in carbon gains (linear model $P = 0.001$, Fig. 3d), resulting in greater losses of aboveground biomass carbon (linear model $P < 0.001$, Fig. 3b). The pre-El Niño baseline temperature was not associated with changes in biomass carbon, nor gains or losses (Fig. 3a,c,e).

Stem mortality rates increased markedly from the pre-El Niño to the El Niño monitoring period by $1.3 \pm 0.4\%$ per year, from 1.8% per year to 3.1% per year (paired t -test, $P < 0.0001$). This occurred in every size class but more so in large (>400 mm diameter, by $1.3 \pm 0.6\%$ per year from 1.4% per year to 2.7% per year, $P < 0.0001$) and medium trees (200–399 mm diameter, by $1.7 \pm 0.5\%$ per year from 1.5% per year to 3.2% per year, $P < 0.0001$), than in small trees (100–199 mm diameter, by $1.1 \pm 0.5\%$ per year from 2.1% to 3.2% per year, $P < 0.0001$). In proportional terms, while mortality rates increased by 50% in the smallest trees, they doubled in the larger size classes. This size-class effect is confirmed by linear mixed effects models, where risk of death during the El Niño was enhanced for the medium and large size classes (Supplementary Table 1). Additionally, trees with greater wood density were at less risk of mortality throughout, and this effect was strengthened during the El Niño. So the El Niño increased risk of death especially for larger trees and for lighter-wooded trees, consistent with expectations from hydraulic failure as a driver of the El Niño enhanced mortality²⁰.

Multi-model inference indicates that drier baseline climates were more important than the temperature anomaly in determining El Niño carbon dynamics impacts, having a slightly larger effect size (Fig. 4). Pre-El Niño baseline climate and El Niño climate anomalies only interact significantly to impact forest carbon gains. Carbon gains are significantly reduced by the interaction of temperature anomaly and drought anomaly, and the interaction of baseline MCWD and drought anomaly (Fig. 4), that is, impacts were exacerbated where it was both hotter and drier. Yet, these significant decreases in carbon gains were too small to be detected in the overall net change analysis, with large carbon losses from mortality tending to dominate the forest responses to El Niño.

Discussion

The 2015–2016 El Niño was the hottest and probably the most extreme drought in South America for at least 50 years^{19,21}. There were high temperatures across the neotropics accompanied by drought anomalies, particularly in south and east Amazonia. Our analysis of long-term field-based records from across tropical South America shows that high temperatures and drought led to increased carbon losses through biomass mortality and that the greatest relative impact of the climate anomalies were in forests where the long-term climate was already relatively dry (Fig. 3).

We might have expected wetter forests to be more vulnerable to climate anomalies as they contain fewer drought-adapted species, and drier forests to be more resistant because they contain more. Yet, our results show that it was exactly where trees are most likely to be pre-adapted to drought that the greatest relative biomass loss was measured. The climatically driest forests were significantly more prone both to El Niño-enhanced carbon losses from biomass mortality and to reduced gains from lower growth and recruitment. Consequently, these drier forests lost biomass during the El Niño period. The drier plots in our dataset were widespread geographically, and we captured the negative carbon impacts of drying in three distinct regions—north Colombia, the Brazilian State of Minas Gerais and the Southern Amazon—including many of the plots both furthest north and furthest south of the equator in our dataset (Fig. 1). These three regions are biogeographically distinct from one another and climatically out of phase, that is, the timings of their wet and dry seasons differ, and yet they exhibited similar negative carbon responses to the climate anomaly. While the potential role of additional factors such as large-scale edge effects

cannot be ruled out^{22,23}, our results point to the limits of pre-adaptation to seasonal climates in conferring resistance to novel climate extremes. Rather than being protected, forests at the dry periphery of the tropical forest biome are especially vulnerable to drought.

During the 2015–2016 El Niño we detected enhanced mortality rates for trees of all sizes. Our results show that over the long term smaller trees experience greater mortality rates. However, the climate anomaly did not just increase the mortality risks for all South American trees, it changed their relative risk in relation to fundamental traits of size and wood density. It drove much greater proportional gains in mortality risk for large and medium-sized trees than it did for trees in the smallest size class, effectively equalizing mortality risks across size classes. Larger trees are inherently more vulnerable to climate extremes because of their size, with greater tension needed to move water longer distances, wider vessels and greater risk of cavitation^{24–26}. Larger trees also may have a more exposed position²⁷ and therefore experience the most extreme temperatures and vapour pressure deficits. In our analyses we find not only a size effect but also that lower wood density trees were more likely to die during the El Niño. Enhanced mortality of larger trees during drought is widely attributed to hydraulic failure^{28,29}, a risk that is greater for fast-growing, lower-wood-density trees^{30,31}. Our results thus show that larger and lighter-wooded trees were more likely to die during the El Niño event, and this is consistent with expectations from increased hydraulic stress.

Our on-the-ground analysis of long-term forest plots revealed that hotter El Niño temperatures increased biomass carbon losses. However, and in contrast to the impact of drought on forests, it was the magnitude of the temperature anomaly itself rather than the temperature baseline that increased carbon losses (Figs. 2 and 3). That the temperature anomaly influences net carbon could be explained by optimization of photosynthesis to local temperature conditions³² and excessive vapour pressure deficits during extreme heat³³.

Before the 2015–2016 El Niño our 123 plots recorded a long-term net increase in aboveground biomass carbon, weighted by sampling effort, of $0.38 \pm 0.16 \text{ Mg C ha}^{-1}$ per year between 2001.4 and 2014.7, indicating a long-term carbon sink. By contrast, during our El Niño monitoring interval the plot net carbon balance declined significantly by $0.40 \pm 0.40 \text{ Mg C ha}^{-1}$ per year to be indistinguishable from zero ($-0.02 \pm 0.37 \text{ Mg C ha}^{-1}$ per year). The net carbon balance also significantly declined in previous droughts in South America, by $0.73 \pm 0.53 \text{ Mg C ha}^{-1}$ per year in 2005 (in 55 monitored plots, data from Phillips et al.¹⁰), and by $0.89 \text{ Mg C ha}^{-1}$ per year ($0.54\text{--}1.26$) in 2010 (in 97 plots, data from Feldpausch et al.¹¹). Comparing our results with the two Amazon drought studies therefore suggests that repeated exposure to drought has caused no loss of intact forest resistance to drought, and although the 2015–2016 El Niño was the hottest drought ever in the Amazon, there is no evidence that its impacts are stronger than those of previous droughts.

Ground observational records of climate anomaly impacts on forests are essential to complement top-down observations and analyses. Our results help inform and interpret large-scale studies that use satellite data measuring related but different processes. We found South American tropical forests to be a carbon sink before the El Niño, which then shut down during the El Niño. Satellite-sensed CO_2 measurements, reflecting net exchange from all processes including productivity, soil and necromass decay, fire and land use change suggest that tropical South America remained a net carbon sink (-0.26 Pg C (-0.58 to 0.04) in 2015 and became a small net source (0.20 Pg C (-0.21 to 0.53) in 2016 (ref. 34). While their combined 2015 and 2016 net balance is similar to our results, the confidence intervals (CIs) are large and the processes being measured are different. Notably, satellites track near real-time carbon losses, while our analysis includes committed losses due to mortality that are not immediately released to the atmosphere, and atmospheric measurements include net soil carbon fluxes, which are not our focus. Another study using satellite-sensed CO_2 estimated

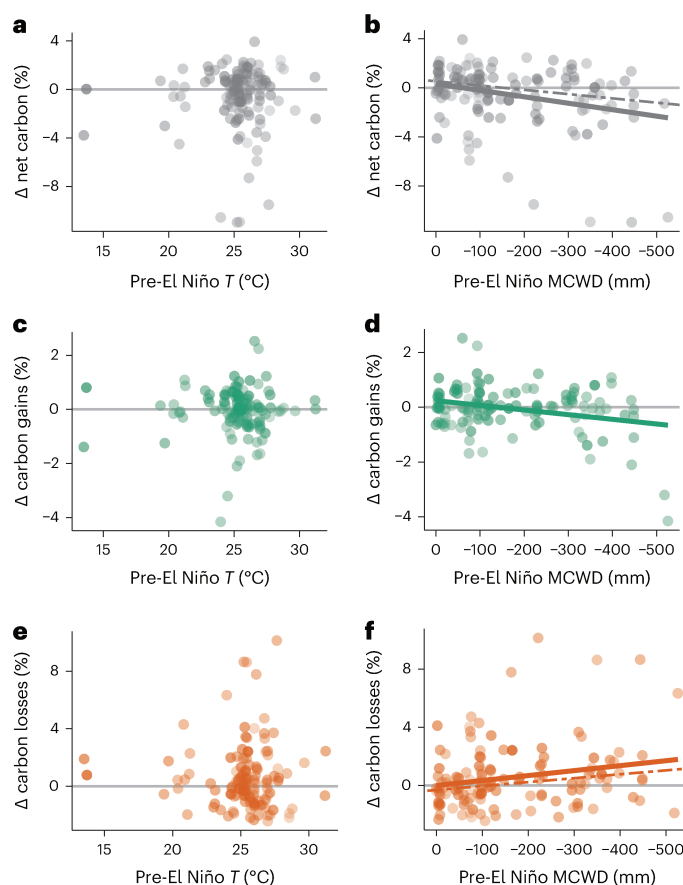


Fig. 3 | Effects of the pre-El Niño climate baseline on aboveground biomass carbon dynamics in 123 neotropical forest plots. a–f, Pre-El Niño temperature (a, c and e) and dry season climate baseline (b, d and f) impacts on aboveground biomass carbon, with forest response variables expressed as relative change. Relative carbon changes are expressed as a percentage of pre-El Niño aboveground biomass carbon at each plot, for example (El Niño carbon gains – pre-El Niño carbon gains)/pre-El Niño aboveground carbon. The net carbon change (a and b), carbon gains from recruitment and growth (c and d) and carbon losses from mortality (e and f) are shown for 123 long-term inventory plots. The pre-El Niño temperature (T) (a, c and e) is the mean of mean monthly temperature in the monitoring period before the El Niño, using the census dates of the plot censuses. The pre-El Niño MCWD (b, d and f) is the mean MCWD in the monitoring period before the El Niño. Point shading from light to dark denotes greater weighting, with plots and line of best fit weighted by an empirically derived combination of pre-El Niño plot monitoring length and plot area for each response variable. Solid lines represent significant linear models ($P < 0.05$) and dashed lines represent significant one-tailed Kendall's τ correlation tests using rank-based linear model estimation ($P < 0.05$). Slopes, intercepts and P values for significant linear models are as follows: B: $y = -0.005x + 0.3$, $P < 0.001$, D: $y = -0.002x + 0.2$, $P = 0.001$, F: $y = 0.003x - 0.002$, $P = 0.02$. See Extended Data Fig. 6 for an alternative analysis excluding censuses before 2000, and Extended Data Fig. 7 for an alternative analysis with carbon changes in absolute terms.

that, compared with the La Niña year of 2011, South American forests had a net emission of 0.9 Pg C due to reduced productivity or higher respiration in 2015 during the El Niño³⁵. Liu et al. (2017) (ref. 35) attribute the apparent decline in growth to lower precipitation, but our ground measurements indicate that drier pre-El Niño baseline climates, as well as the temperature anomaly, reduced net carbon via increased aboveground biomass mortality rather than reducing biomass growth (Fig. 4). Other ground measurements, including disturbed forests unlike ours, indicate that mortality rates remained elevated for up to 3 years following the climate anomaly, with fires responsible for much of the biomass mortality³⁶.

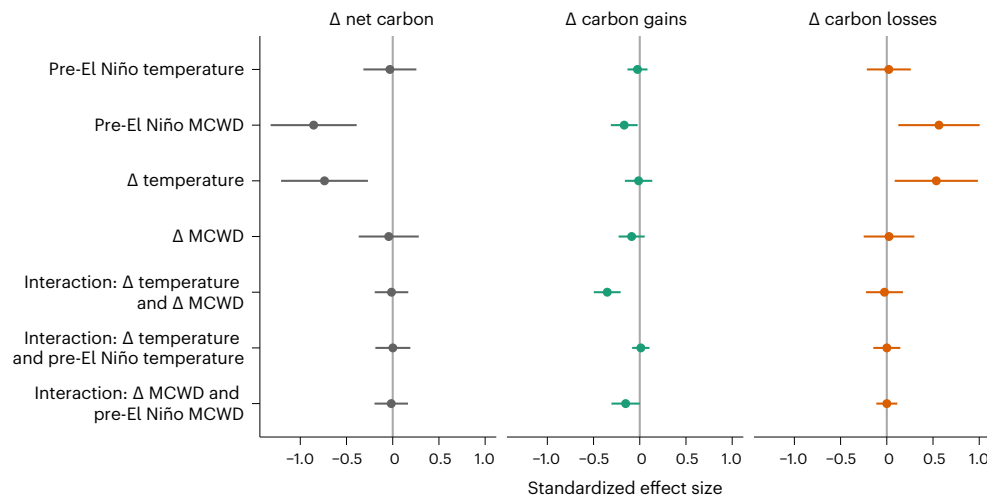


Fig. 4 | Standardized effect sizes of change in relative aboveground biomass carbon in South American tropical forests over the 2015–2016 El Niño.

Points show coefficients from model-averaged linear models, $n = 123$ plots, and error bars show 95% CIs, centred on the mean. Variables that did not occur in well-supported models are shrinkage adjusted towards zero. Coefficients are standardized so that they represent change in the response variable for one

standard deviation change in the explanatory variable. The full models explained 18%, 31% and 12% of variation in Δ net carbon, Δ carbon gains and Δ carbon losses. Equations for models are listed in Supplementary Table 2. See Extended Data Fig. 8 for an alternative analysis excluding censuses before 2000, and Extended Data Fig. 9 for an alternative analysis with carbon changes in absolute terms.

We can also use the relative impacts of the El Niño climate anomaly on the net carbon sink to estimate scaled-up carbon impacts from our ground measurements. A recent assessment of the long-term biomass carbon sink in South American forests reports a value of 0.45 Pg C per year (0.31–0.57, 95% CIs) for the years 2000 to 2010 (ref. 8). Our results suggest that the net sink was reduced by 105% during the El Niño interval. So, over the 2.7 year period we estimate a net biomass loss of only 0.02 Pg C per year (that is, –105% of 0.45 Pg C per year). However, our 2.7 year census window captures months of more normal climate in addition to the El Niño climate anomaly, and we may assume that the climate impacts on forest dynamics were concentrated within the 12 months of extreme climate. If this were the case, we estimate a carbon source of 0.82 Pg C for the El Niño year itself. During the same El Niño event, comparatively resistant African tropical forests continued to be a carbon sink over the period they were measured, with a sink decline of only 36%, and no strong carbon source even when estimated over the 12 months of climate anomaly³⁷. South American tropical forests therefore appear to be more sensitive to El Niño events than African forests.

By measuring the impacts of the most extreme climate event yet recorded in tropical South America and relating them to long-term forest records from the same sites, sustained ground measurements have provided unique insight into its impacts and helped quantify forest sensitivity to climate change. Our analysis suggests that many South American forests are vulnerable to temperature increases, and that the drier forests in particular are most vulnerable to climate change. Rather than being protected through long-term adaptation, forests at the dry periphery of the tropical forest biome are more vulnerable to extreme events. Yet, although the 2015–2016 El Niño was the hottest drought ever in the Amazon, and was exceptionally dry, our long-term on-the-ground measurements show that its impacts were no greater than those of previous droughts. These undisturbed forests were no more sensitive to recent climate extremes than previous, less intense climate events. Intact South American tropical forests have hence demonstrated the capacity to resist climate change so far, further strengthening the case for their conservation as a key defence against climate change.

Inclusion and ethics

ForestPlots.net is a global community of researchers striving to make long-term plot monitoring more equitable. Our partners independently

access, analyse and manage the information from their own plots, and can choose to join and initiate their own collaborative projects across countries and continents. We seek to ensure that both the production and the use of forest data becomes more equitable, that the many less-visible colleagues who contribute vital work receive proper recognition, and that we support fair, long-term collaboration across geographical, socio-economic and cultural divides. Further information on how we promote sustainable and equitable collaborations among researchers is set out in the Code of Conduct³⁸.

Online content

Any methods, additional references, Nature Portfolio reporting summaries, source data, extended data, supplementary information, acknowledgements, peer review information; details of author contributions and competing interests; and statements of data and code availability are available at <https://doi.org/10.1038/s41558-023-01776-4>.

References

- Pan, Y. et al. A large and persistent carbon sink in the world's forests. *Science* **333**, 988–993 (2011).
- Booth, B. B. B. et al. High sensitivity of future global warming to land carbon cycle processes. *Environ. Res. Lett.* **7**, 024002 (2012).
- Lewis, S. L., Edwards, D. P. & Galbraith, D. Increasing human dominance of tropical forests. *Science* <https://doi.org/10.1126/science.aaa9932> (2015).
- Koch, A., Hubau, W. & Lewis, S. L. Earth System Models are not capturing present-day tropical forest carbon dynamics. *Earth's Future* <https://doi.org/10.1029/2020EF001874> (2021).
- Pan, Y., Birdsey, R. A., Phillips, O. L. & Jackson, R. B. The structure, distribution, and biomass of the world's forests. *Annu. Rev. Ecol. Syst.* **44**, 593–622 (2013).
- ter Steege, H. et al. Hyperdominance in the Amazonian tree flora. *Science* **342**, 6156 (2013).
- Brienen, R. J. W. et al. Long-term decline of the Amazon carbon sink. *Nature* **519**, 344–348 (2015).
- Hubau, W. et al. Asynchronous carbon sink saturation in African and Amazonian tropical forests. *Nature* **579**, 80–87 (2020).
- Aleixo, I. et al. Amazonian rainforest tree mortality driven by climate and functional traits. *Nat. Clim. Chang.* **9**, 384–388 (2019).

10. Phillips, O. L. et al. Drought sensitivity of the Amazon rainforest. *Science* **323**, 1344–1347 (2009).
11. Feldpausch, T. R. et al. Amazon forest response to repeated droughts. *Glob. Biogeochem. Cycles* <https://doi.org/10.1002/2015GB005133> (2016).
12. Maia, V. A. et al. The carbon sink of tropical seasonal forests in southeastern Brazil can be under threat. *Sci. Adv.* **6**, eabd4548 (2020).
13. Gatti, L. V. et al. Amazonia as a carbon source linked to deforestation and climate change. *Nature* **595**, 388–393 (2021).
14. Araújo, I. et al. Trees at the Amazonia–Cerrado transition are approaching high temperature thresholds. *Environ. Res. Lett.* **16**, 034047 (2021).
15. Harris, N. L. et al. Global maps of twenty-first century forest carbon fluxes. *Nat. Clim. Chang.* **11**, 234–240 (2021).
16. McDowell, N. et al. Drivers and mechanisms of tree mortality in moist tropical forests. *N. Phytol.* **219**, 851–869 (2018).
17. Doughty, C. E. & Goulden, M. L. Are tropical forests near a high temperature threshold? *J. Geophys. Res.* <https://doi.org/10.1029/2007JG000632> (2008).
18. Allen, K. et al. Will seasonally dry tropical forests be sensitive or resistant to future changes in rainfall regimes? *Environ. Res. Lett.* **12**, 023001 (2017).
19. Jiménez-Muñoz, J. C. et al. Record-breaking warming and extreme drought in the Amazon rainforest during the course of El Niño 2015–2016. *Sci. Rep.* **6**, 33130 (2016).
20. Tavares, J. V. et al. Basin-wide variation in tree hydraulic safety margins predicts the carbon balance of Amazon forests. *Nature* **617**, 111–117 (2023).
21. Panisset, J. S. et al. Contrasting patterns of the extreme drought episodes of 2005, 2010 and 2015 in the Amazon Basin. *Int. J. Climatol.* **38**, 1096–1104 (2018).
22. Ferreira, L. V. & Laurance, W. F. Effects of forest fragmentation on mortality and damage of selected trees in Central Amazonia. *Conserv. Biol.* **11**, 797–801 (1997).
23. Reis, S. M. et al. Climate and fragmentation affect forest structure at the southern border of Amazonia. *Plant Ecol. Divers.* **11**, 13–25 (2018).
24. McDowell, N. G. & Allen, C. D. Darcy’s law predicts widespread forest mortality under climate warming. *Nat. Clim. Change* **5**, 669–672 (2015).
25. Olson, M. E. et al. Plant height and hydraulic vulnerability to drought and cold. *Proc. Natl Acad. Sci. USA* **115**, 7551–7556 (2018).
26. Mencuccini, M. et al. Size-mediated ageing reduces vigour in trees. *Ecol. Lett.* **8**, 1183–1190 (2005).
27. McGregor, I. R. et al. Tree height and leaf drought tolerance traits shape growth responses across droughts in a temperate broadleaf forest. *N. Phytol.* **231**, 601–616 (2021).
28. Rowland, L. et al. Death from drought in tropical forests is triggered by hydraulics not carbon starvation. *Nature* **528**, 119–122 (2015).
29. Gora, E. M. & Esquivel-Muelbert, A. Implications of size-dependent tree mortality for tropical forest carbon dynamics. *Nat. Plants* **7**, 384–391 (2021).
30. Oliveira, R. S. et al. Linking plant hydraulics and the fast–slow continuum to understand resilience to drought in tropical ecosystems. *N. Phytol.* **230**, 904–923 (2021).
31. Eller, C. B. et al. Xylem hydraulic safety and construction costs determine tropical tree growth. *Plant Cell Environ.* **41**, 548–562 (2018).
32. Slot, M. & Winter, K. In situ temperature response of photosynthesis of 42 tree and liana species in the canopy of two Panamanian lowland tropical forests with contrasting rainfall regimes. *N. Phytol.* **214**, 1103–1117 (2017).
33. Bauman, D. et al. Tropical tree mortality has increased with rising atmospheric water stress. *Nature* **608**, 528–533 (2022).
34. Palmer, P. I. et al. Net carbon emissions from African biosphere dominate pan-tropical atmospheric CO₂ signal. *Nat. Commun.* **10**, 3344 (2019).
35. Liu, J. et al. Contrasting carbon cycle responses of the tropical continents to the 2015–2016 El Niño. *Science* **358**, eaam5690 (2017).
36. Berenguer, E. et al. Tracking the impacts of El Niño drought and fire in human-modified Amazonian forests. *Proc. Natl Acad. Sci. USA* **118**, e2019377118 (2021).
37. Bennett, A. C. et al. Resistance of African tropical forests to an extreme climate anomaly. *Proc. Natl Acad. Sci. USA* **118**, e2003169118 (2021).
38. ForestPlots.net. Code of conduct. (School of Geography, Univ. of Leeds, 2023); <https://forestplots.net/en/join-forestplots/code-of-conduct>

Publisher’s note Springer Nature remains neutral with regard to jurisdictional claims in published maps and institutional affiliations.

Open Access This article is licensed under a Creative Commons Attribution 4.0 International License, which permits use, sharing, adaptation, distribution and reproduction in any medium or format, as long as you give appropriate credit to the original author(s) and the source, provide a link to the Creative Commons license, and indicate if changes were made. The images or other third party material in this article are included in the article’s Creative Commons license, unless indicated otherwise in a credit line to the material. If material is not included in the article’s Creative Commons license and your intended use is not permitted by statutory regulation or exceeds the permitted use, you will need to obtain permission directly from the copyright holder. To view a copy of this license, visit <http://creativecommons.org/licenses/by/4.0/>.

© The Author(s) 2023

Amy C. Bennett¹✉, Thaiane Rodrigues de Sousa², Abel Monteagudo-Mendoza³, Adriane Esquivel-Muelbert^{4,5}, Paulo S. Morandi⁶, Fernanda Coelho de Souza⁷, Wendeson Castro⁸, Luisa Fernanda Duque⁹, Gerardo Flores Llampazo¹⁰, Rubens Manoel dos Santos¹¹, Eliana Ramos¹², Emilio Vilanova Torre¹³, Esteban Alvarez-Davila^{14,15}, Timothy R. Baker¹, Flávia R. C. Costa¹², Simon L. Lewis^{1,16}, Beatriz S. Marimon⁶, Juliana Schiatti¹⁷, Benoît Burban¹⁸, Erika Berenguer^{19,20}, Alejandro Araujo-Murakami²¹, Zorayda Restrepo Correa⁹, Wilmar Lopez^{22,23}, Flávia Delgado Santana¹², Laura Jessica Viscarra²¹, Fernando Elias²⁴, Rodolfo Vasquez Martinez³, Ben Hur Marimon-Junior²⁵, David Galbraith¹, Martin J. P. Sullivan²⁶, Thaise Emilio²⁷, Nayane C. C. S. Prestes⁶, Jos Barlow²⁰, Nathalie Cristine Alencar Fagundes¹¹, Edmar Almeida de Oliveira⁶, Patricia Alvarez Loayza²⁸, Luciana F. Alves²⁹, Simone Aparecida Vieira³⁰, Vinícius Andrade Maia¹¹, Luiz E. O. C. Aragão^{31,32}, Eric J. M. M. Arets³³, Luzmila Arroyo³⁴, Olaf Bánki³⁵, Christopher Baraloto³⁶, Plínio Barbosa Camargo³⁷, Jorcely Barroso³⁸, Wilder Bento da Silva¹¹, Damien Bonal³⁹, Alisson Borges Miranda Santos¹¹, Roel J. W. Brienen¹,

Foster Brown⁴⁰, Carolina V. Castilho⁴¹, Sabina Cerruto Ribeiro⁴², Victor Chama Moscoso^{3,43}, Ezequiel Chavez⁴⁴, James A. Comiskey^{45,46}, Fernando Cornejo Valverde⁴⁷, Nállarett Dávila Cardozo⁴⁸, Natália de Aguiar-Campos¹¹, Lia de Oliveira Melo⁴⁹, Jhon del Aguila Pasquel^{50,51}, Géraldine Derroire⁵², Mathias Disney^{16,53}, Maria do Socorro, Aurélie Dourdain⁵², Ted R. Feldpausch³², Joice Ferreira⁵⁴, Valeria Forni Martins^{27,55}, Toby Gardner⁵⁶, Emanuel Gloor¹, Gloria Gutierrez Sibauty⁵⁷, René Guillen⁵⁸, Eduardo Hase², Bruno Hérault^{59,60}, Eurídice N. Honorio Coronado⁶¹, Walter Huaraca Huasco⁶², John P. Janovec⁶³, Eliana Jimenez-Rojas⁶⁴, Carlos Joly²⁷, Michelle Kalamandeen^{65,66}, Timothy J. Killeen⁶⁷, Camila Lais Farrapo¹¹, Aurora Levesley¹, Leon Lizon Romano^{54,68,69}, Gabriela Lopez Gonzalez¹, Flavio Antonio Maës dos Santos²⁷, William E. Magnusson⁷⁰, Yadvinder Malhi¹⁹, Simone Matias de Almeida Reis^{6,8,19}, Karina Melgaço¹, Omar A. Melo Cruz⁷¹, Irina Mendoza Polo⁷², Tatiana Montañez⁷¹, Jean Daniel Morel¹¹, M Percy Núñez Vargas⁶², Raimunda Oliveira de Araújo², Nadir C. Pallqui Camacho^{1,62}, Alexander Parada Gutierrez⁷³, Toby Pennington³², Georgia C. Pickavance¹, John Pipoly^{74,75}, Nigel C. A. Pitman⁷⁶, Carlos Quesada², Freddy Ramirez Arevalo⁴⁸, Hirma Ramírez-Angulo⁷⁷, Rafael Flora Ramos³⁰, James E. Richardson^{78,79,80,81}, Cléber Rodrigo de Souza^{11,82}, Anand Roopsind⁸³, Gustavo Schwartz⁸⁴, Richarlly C. Silva⁴², Javier Silva Espejo⁶², Marcos Silveira⁴², James Singh⁸⁵, Yhan Soto Shareva³, Marc Steininger⁸⁶, Juliana Stropp⁸⁷, Joey Talbot^{1,88}, Hans ter Steege^{35,89}, John Terborgh^{90,91}, Raquel Thomas⁹², Luis Valenzuela Gamarra³, Geertje van der Heijden⁹³, Peter van der Hout⁹⁴, Roderick Zagt⁹⁵ & Oliver L. Phillips¹

¹School of Geography, University of Leeds, Leeds, UK. ²Instituto Nacional de Pesquisas da Amazônia (INPA), Manaus, Brazil. ³Jardín Botánico de Missouri, Oxapampa, Peru. ⁴School of Geography, Earth and Environmental Sciences, University of Birmingham, Birmingham, UK. ⁵Birmingham Institute of Forest Research, BIFoR, University of Birmingham, Birmingham, UK. ⁶UNEMAT—Universidade do Estado de Mato Grosso, Nova Xavantina, Brazil. ⁷Department of Forestry, University of Brasília, Campus Darcy Ribeiro, Brasília, Brazil. ⁸Universidade Federal do Acre, Rio Branco, Brazil. ⁹Socioecossistemas y Cambio Climático, Fundación Con Vida, Medellín, Colombia. ¹⁰Universidad Nacional Jorge Basadre de Grohmann, Tacna, Peru. ¹¹Laboratório de Fitogeografia e Ecologia Evolutiva, Universidade Federal de Lavras, Lavras, Brazil. ¹²Instituto Nacional da Mata Atlântica, Santa Teresa, Brasil. ¹³Wildlife Conservation Society, Bronx, NY, USA. ¹⁴Escuela de Ciencias Agrícolas, Pecuarias y del Medio Ambiente, National Open University and Distance, Bogotá, Colombia. ¹⁵Fundación Con Vida, Medellín, Colombia. ¹⁶Department of Geography, University College London, London, UK. ¹⁷Universidade Federal do Amazonas (UFAM), Manaus, Brazil. ¹⁸INRAE, UMR EcoFoG (AgroParisTech, CNRS, INRAE, Université des Antilles, Université de Guyane), Kourou, French Guiana. ¹⁹Environmental Change Institute, School of Geography and the Environment, University of Oxford, Oxford, UK. ²⁰Lancaster Environment Centre, Lancaster University, Lancaster, UK. ²¹Museo de Historia Natural Noel Kempff Mercado, Universidad Autónoma Gabriel René Moreno, Santa Cruz, Bolivia. ²²Escuela de Estadística, Facultad de Ciencias, Universidad Nacional de Colombia, Medellín, Colombia. ²³Departamento de Ciencias Forestales, Facultad de Ciencias Agrarias, Universidad Nacional de Colombia, Medellín, Colombia. ²⁴Institute of Biological Sciences, Universidade Federal do Pará, Belém, Brazil. ²⁵Faculdade de Ciências Agrárias, Biológicas e Sociais Aplicadas, UNEMAT - Universidade do Estado de Mato Grosso, Nova Xavantina, Brazil. ²⁶Department of Natural Sciences, Manchester Metropolitan University, Manchester, UK. ²⁷Programa Nacional de Pós-Doutorado (PNPD), Programa de Pós-Graduação em Ecologia, Institute of Biology, University of Campinas (UNICAMP), Campinas, Brazil. ²⁸Nicholas School of the Environment, Duke University, Durham, NC, USA. ²⁹Center for Tropical Research, Institute of the Environment and Sustainability, University of California, Los Angeles, CA, USA. ³⁰Universidade Estadual de Campinas, Campinas, Brazil. ³¹National Institute for Space Research (INPE), São José dos Campos, Brazil. ³²Geography, College of Life and Environmental Sciences, University of Exeter, Exeter, UK. ³³Wageningen Environmental Research, Wageningen University & Research, Wageningen, the Netherlands. ³⁴Dirección de la Carrera de Biología, Universidad Autónoma Gabriel René Moreno, Santa Cruz, Bolivia. ³⁵Naturalis Biodiversity Center, Leiden, the Netherlands. ³⁶Institute of Environment, Department of Biological Sciences, Florida International University, Miami, FL, USA. ³⁷Centro de Energia Nuclear na Agricultura, Universidade de São Paulo, São Paulo, Brazil. ³⁸Centro Multidisciplinar, Universidade Federal do Acre, Cruzeiro do Sul, Brazil. ³⁹Université de Lorraine, INRAE, UMR Silva, AgroParisTech, Nancy, France. ⁴⁰Woods Hole Research Center, Falmouth, MA, USA. ⁴¹Embrapa Roraima, Brazilian Agricultural Research Corporation (EMBRAPA), Boa Vista, Brazil. ⁴²Centro de Ciências Biológicas e da Natureza, Universidade Federal do Acre, Rio Branco, Brazil. ⁴³Universidad Nacional San Antonio Abad del Cusco, Cusco, Peru. ⁴⁴Museo Noel Kempff, Santa Cruz, Bolivia. ⁴⁵Inventory and Monitoring Program, National Park Service, Fredericksburg, VA, USA. ⁴⁶Smithsonian Institution, Washington, DC, USA. ⁴⁷Proyecto Castaña, Madre de Dios, Peru. ⁴⁸Facultad de Ciencias Biológicas, Universidad Nacional de la Amazonia Peruana, Iquitos, Peru. ⁴⁹Universidade Federal do Oeste do Para, Santarem, Brazil. ⁵⁰Instituto de Investigaciones de la Amazonia Peruana, Iquitos, Peru. ⁵¹Universidad Nacional de la Amazonia Peruana, Iquitos, Peru. ⁵²Cirad, UMR EcoFoG (AgroParisTech, CNRS, INRAE, Université des Antilles, Université de Guyane), Kourou, French Guiana. ⁵³NERC National Centre for Earth Observation (NCEO), Leicester, UK. ⁵⁴Embrapa Amazônia Oriental, Brazilian Agricultural Research Corporation (EMBRAPA), Brasília, Brazil. ⁵⁵Department of Natural Sciences, Maths and Education, Centre for Agrarian Sciences, Federal University of São Carlos (UFSCar), Araras, Brazil. ⁵⁶Stockholm Environment Institute, Stockholm, Sweden. ⁵⁷Jardín Botánico Municipal de Santa Cruz, Santa Cruz, Bolivia. ⁵⁸Parque Nacional y Área Natural de Manejo Integrado 'Kaa-iyá del Gran Chaco', Santa Cruz, Bolivia. ⁵⁹CIRAD, UPR Forêts et Sociétés, Montpellier, France. ⁶⁰Forêts et Sociétés, Univ Montpellier, CIRAD, Montpellier, France. ⁶¹School of Geography and Sustainable Development, University of St Andrews, St Andrews, UK. ⁶²Universidad Nacional San Antonio Abad de Cusco, Cusco, Peru. ⁶³Herbario Forestal UNALM, Facultad de Ciencias Forestales, Universidad Nacional Agraria La Molina, Lima, Peru. ⁶⁴Instituto IMANI, Universidad Nacional de Colombia, Leticia, Colombia. ⁶⁵Department of Plant Sciences, University of Cambridge, Cambridge, UK. ⁶⁶Living with Lakes Centre, Laurentian University, Sudbury, Ontario, Canada. ⁶⁷Museo de Historia Natural Noel Kempff Mercado, Santa Cruz, Bolivia. ⁶⁸Universidade Federal do Pará, Belém, Brazil. ⁶⁹Museu Paraense Emílio Goeldi, Belém, Brazil. ⁷⁰Coordenação da Biodiversidade, Instituto Nacional de Pesquisas da Amazônia (INPA), Manaus, Brazil. ⁷¹Universidad del Tolima, Ibagué, Colombia. ⁷²Grupo de Investigación en Servicios Ecosistémicos y Cambio Climático, Jardín Botánico de Medellín, Medellín, Colombia. ⁷³UNELLEZ-Guanare, Programa de Ciencias del Agro y el Mar, Herbario Universitario (PORT), Barinas, Venezuela. ⁷⁴Broward County Parks & Recreation, Oakland Park, FL, USA. ⁷⁵Florida Atlantic University, Boca Raton, FL, USA. ⁷⁶Keller Science Action Center, Field Museum, Chicago, IL, USA. ⁷⁷Universidad de Los Andes, Mérida, Venezuela. ⁷⁸School of Biological, Earth and Environmental Sciences, University College Cork, Cork, Ireland. ⁷⁹Departamento de Biología, Facultad de Ciencias Naturales, Universidad del Rosario, Bogotá, Colombia. ⁸⁰Tropical Diversity Section, Royal Botanic Garden Edinburgh, Edinburgh, UK. ⁸¹The Environmental Research Institute, University

College Cork, Cork, Ireland. ⁸²Carbon Serviços Ambientais, Piracicaba, Brazil. ⁸³Conservation International, Arlington, VA, USA. ⁸⁴Embrapa Amazônia Oriental, Brazilian Agricultural Research Corporation (EMBRAPA), Belém, Brazil. ⁸⁵Guyana Forestry Commission, Georgetown, Guyana. ⁸⁶Department of Geographical Sciences, University of Maryland, College Park, MD, USA. ⁸⁷Departamento de Biogeografía y Cambio Global, Museo Nacional de Ciencias Naturales, Consejo Superior de Investigaciones Científicas (MNCN-CSIC), Madrid, Spain. ⁸⁸Institute for Transport Studies, University of Leeds, Leeds, UK. ⁸⁹Quantitative Biodiversity Dynamics, Department of Biology, Utrecht University, Utrecht, the Netherlands. ⁹⁰Florida Museum of Natural History and Department of Biology, University of Florida, Gainesville, FL, USA. ⁹¹School of Science and Engineering, James Cook University, Cairns, Queensland, Australia. ⁹²Iwokrama International Centre for Rainforest Conservation and Development, Georgetown, Guyana. ⁹³School of Geography, University of Nottingham, Nottingham, UK. ⁹⁴Van der Hout Forestry Consulting, Rotterdam, the Netherlands. ⁹⁵Tropenbos International, Ede, the Netherlands.

✉ e-mail: acrbennett@gmail.com

Methods

Plot data collection and analysis

All long-term forest inventory plots analysed are lowland, closed canopy, mature tropical forests, had been censused at least twice before the 2015–2016 El Niño event and were censused at least once afterwards. To be included in the analysis plots must also have had no more than 5 years between the census immediately before the El Niño and the census following the El Niño, and these censuses must also have taken place in the same season (within 120 days). We inspected the temperature and cumulative water deficits of the months between censuses to determine which census interval captured the climate extremes of the El Niño for that plot. Any additional censuses after the El Niño census were not used in this analysis. The El Niño plot census interval should capture maximum drought, and, because MCWD is a lagging metric with deficits cumulated to the end of the month, we use the final pre-El Niño census month as the conditions at the start of the El Niño interval. Ideally, and in most cases, the census interval captures peak temperature as well as maximum drought, but in a few plots with shorter El Niño census intervals only one climate extreme is captured by the El Niño census interval, and that was usually drought.

The 123 plots meeting these criteria are distributed across 50 distinct clusters in six countries: Bolivia, Brazil, Colombia, French Guiana, Peru and Venezuela. Fourteen Brazilian plots are in the PPBio network³⁹; the remaining 109 plots contribute to the RAINFOR network⁴⁰. While some plots were established as early as 1962, to avoid potential impacts of the 1982–1983 El Niño event, we include only censuses after 1983. The plot median size was 1 ha, and the mean 1.05 ha (range 0.25–6.25 ha). The mean initial census date was May 2001, mean pre-El Niño census was September 2014 and mean post-El Niño census was May 2017. The mean pre-El Niño monitoring length was 13.3 years and the mean length of the El Niño interval was 2.7 years. We checked that temporal consistency among plot censuses was adequate by repeating our analysis only with a shorter baseline, excluding censuses before 2000. These alternative analyses yielded similar results and are available in the extended data (with Extended Data Figs. 4–9 directly comparable to Figs. 2–4). All data are curated at ForestPlots.net⁴¹ version 2020.1 downloaded on 19 October 2020, data and code associated with the analyses can be accessed using ref. 42. For plot details, see Supplementary Tables 3 and 4.

In each plot, all trees ≥ 100 mm diameter were measured, tagged with a unique identifier and identified to species, where possible. Tree diameter was measured at 1.3 m along the stem from the ground, or above buttresses, if present, using standardized methods for all plots⁴³. In some cases, the point of diameter measurement had to be moved due to upward growth of buttresses or deformities. For these trees, we calculated a single common estimate of growth before and after the point of diameter measurement change^{8,44–47}. Stems that reached a diameter ≥ 100 mm during the census interval were recorded as new recruits.

Field data were checked against rules to identify potential errors, identically for all 123 plots, consistent with previous large-scale analyses^{7,8,44,48}. We assessed trees that increased in diameter >40 mm per year or shrunk >5 mm over an interval, to determine if they could have been inaccurately measured in the field. For example, fast-growing species in a canopy gap could grow >40 mm per year, or a rotten trunk could shrink >5 mm in an interval, but for those deemed potentially inaccurate the diameter was either interpolated or extrapolated using known measurements from the same stem from other censuses. When only one accurate measurement was available, growth was estimated by applying the mean growth rate (for diameter classes 100–199 mm and 200–399 mm) or median growth rate, for size classes with few stems (for diameters 400+ mm) (0.4% of all measurements).

We estimated tree aboveground mass using the following allometric equation⁴⁹:

$$\text{AGB} = 0.0673 \times (\rho D^2 H)^{0.976},$$

where ρ is stem wood density (g cm^{-3}), D is stem diameter (cm) at 1.3 m or above buttresses, and H is height (m). We estimate the above-ground mass of palms using the equation in Goodman et al. (2013) (ref. 50). Wood density measurements were compiled mostly from the Global Wood Density Database on the Dryad digital repository (datadryad.org)^{51,52} and each individual stem in a plot was matched to a species-specific mean wood density value, where possible. For incompletely identified individuals or individuals belonging to species not in the wood density database, we use the mean wood density value for genus if available, then family. For unidentified individuals, we used the mean wood density value of all individual trees in the plot^{47,53}.

Tree heights were measured in 108 plots; typically the 10 largest trees and 10 trees in each of the diameter classes 100–199 mm, 200–299 mm, 300–399 mm, 400–499 mm and 500–599 mm, with trees selected only when the top was visible⁵⁴. To estimate height for plots or trees a three-parameter regional height-diameter Weibull equation was fitted using the local heights function in the BiomasaFPR package⁵⁵. The regions were Amazonia: Brazilian Shield, East-Central, Guiana Shield and West, and the parameters were used to estimate tree height from tree diameter for all stems for input into the allometric equation.

We estimated the aboveground biomass in live stems (AGB), in Mg dry mass ha^{-1} , at each census of each plot; the additions of biomass to each plot over the census interval, as aboveground wood productivity (AGWP), in Mg dry mass ha^{-1} per year, and the losses of AGB from the plot, termed AGB mortality, also in Mg dry mass ha^{-1} per year. Plot-level carbon gains and losses are increasingly underestimated as census length increases, so to avoid census-interval effects we corrected using the method outlined in Talbot et al.⁴⁶. We thus accounted for the carbon additions from trees that recruited and then died within the same interval (unobserved recruitment), and the carbon additions from trees that grew before they died within an interval (unobserved growth). Carbon losses are affected by similar processes, so we added the estimated growth before tree death within the interval (unobserved growth), and the deaths of stems that were newly recruited within the interval (unobserved mortality).

We used the BiomasaFPR package to calculate AGB, AGWP and AGB mortality, including the calculation of the census interval corrections. Pre-El Niño means of these variables are time-weighted on the basis of the census interval lengths. Where AGB, AGWP and AGB mortality are expressed in carbon terms (net change in carbon stocks, carbon gains and carbon losses) we use the mean carbon fraction for tropical angiosperms, 45.6% (ref. 56). The difference between the mean of the pre-El Niño monitoring period and the mean of the El Niño census interval is Δ net carbon, Δ carbon gains and Δ carbon losses for each plot. We report results in terms of relative biomass carbon impacts as a percentage of initial aboveground plot carbon as we are comparing a wide range of forests, but have also analysed absolute impacts which show similar trends (Extended Data Figs. 5, 7 and 9).

We weighted the plots when testing the impacts of climate (temperature and MCWD) on biomass carbon (Δ net carbon, Δ carbon gains and Δ carbon losses) using linear regression because larger plots and those monitored for longer are expected to provide better estimates of changes in carbon, carbon gains and carbon losses. We calculate an empirical optimum weighting using plot area and pre-El Niño monitoring length, by assuming a priori that there is no pattern in the change in carbon, carbon gains or carbon losses. We assessed the patterns in the residuals of sampling effort versus change in carbon, carbon gains and carbon losses following different weightings to remove any pattern in the residuals⁴⁷. Selected weights were: Δ net carbon, $\text{Area}^{1/2} + \text{monitoring length}^{1/3} - 1$; Δ carbon gains, $\text{Area}^{1/7} + \text{monitoring length}^{1/7} - 1$; Δ carbon losses, $\text{Area}^{1/3} + \text{monitoring length}^{1/4} - 1$. Instantaneous stem mortality rates were calculated and corrected for census interval effects using equation 3 from Lewis et al.⁵⁷.

We used linear models, Kendall's τ correlation tests and rank-based regression lines of best fit to determine significant relationships

between carbon dynamics and climate. Rank based regression lines were plotted using the `rfit` function from the `Rfit` R package⁵⁸. We checked whether the explanatory climate variables covary, and as a rule of thumb we assumed correlations above 0.7 should not be included in multiple regression⁵⁹. Multicollinearity was not an issue as correlation coefficients between explanatory variables were low ($r < 0.24$) and variance inflation factors from fitted models were ≤ 1.4 , and thus well below the common cut-off of 5 (ref. 60), allowing us to include them in multiple regression. Mixed effects models of factors associated with tree death were performed using the `glmer` function from the `lme4` R package⁶¹.

The multiple linear models test the impacts of pre-El Niño climate (pre-El Niño temperature and pre-El Niño MCWD) and climate anomaly (Δ temperature, Δ MCWD and their interaction) on biomass carbon (Δ net carbon, Δ carbon gains and Δ carbon losses) (full model equations listed in Supplementary Table 1). We included pre-El Niño climate in our models to test whether plots that were already hotter (pre-El Niño temperature) or plots that were already drier (pre-El Niño MCWD) were more or less resistant to climate extremes (trees in hotter or drier pre-El Niño climates may contain more hot or dry adapted species, but also may be closer to physiological temperature or moisture thresholds). We include interactions in our models as we might expect greater impacts in locations that are hotter pre-El Niño and experience a greater temperature anomaly (pre-El Niño temperature interacts with Δ temperature), or locations that are drier pre-El Niño and experience a greater MCWD anomaly (pre-El Niño MCWD interacts with Δ MCWD), and high temperatures may exacerbate water deficits (Δ temperature interacts with Δ MCWD). Variables were standardized to allow effect size comparisons. Global models with all possible combinations (subsets) of effect terms were restricted to a 95% confidence set (Akaike information criterion weights of models sum to 0.95), thereby excluding highly unlikely models. We then model averaged the coefficients of terms (using the Akaike information criterion weights of each model), meaning terms with limited support exhibit shrinkage towards zero⁶². Multi-model inference was performed using the `dredge` and `model.avg` functions of the `MuMIn` R package⁶³.

Climate analysis

Temperature, precipitation and drought estimation. We required a continuous climate record from 1970 to 2018 over South American forests, which meant combining products with different timespans and scales. We used (1) the mean monthly 2 m temperature (30 km resolution) from the ERA5 dataset for 1979 to 2018 (ref. 64) and (2) monthly temperature (0.5° resolution) from the Climate Research Unit (CRU) ts.4.03 dataset for 1970–1978 (ref. 65). The CRU dataset was resampled to match the resolution of ERA5 and harmonized to Celsius units. For each month of the overlapping period ERA5 and CRU we plotted the regression of CRU on ERA5 (1979–2018, that is, January CRU versus January ERA5) for all neotropical forest pixels, and the fit was used to correct the CRU data to match ERA5. The 1970 to 2018 temperature record (T) includes the monthly adjusted CRU data (1970 to 1978) and monthly ERA5 data from 1979 to 2018.

For temperature data at a finer spatial resolution, we also down-scaled our temperature data to 1 km² using WorldClim v2 (ref. 66) by first resampling the 1970–2018 temperature record to match the resolution of WorldClim. We then use the static 1970–2000 WorldClim temperature to correct the 1970–2018 record for each plot location by calculating the mean monthly temperature (μ) for the CRU-ERA-1 record for the period 1970–2000. The monthly difference ($T_{\text{diff}} = T_{\mu} - T_{\text{WorldClim}}$) of the mean climate, T_{diff} was then used to create a plot-level monthly temperature 1970–2017: $T_{\text{plot}} = T - T_{\text{diff}}$. Temperature values were then additionally adjusted for any difference in altitude between the plot and the altitude of the 1 km grid cell used for WorldClim interpolation, using a lapse rate, so that $T_{\text{plotalt}} = T_{\text{plot}} + 0.005 \times (A_{\text{WorldClim}} - A_{\text{plot}})$, where T is temperature (°C) and A is altitude (m).

Similarly, continuous precipitation records were required from 1970 to 2018. We used (1) monthly precipitation (0.25° resolution) from the Tropical Rainfall Measurement Mission (TRMM product 3B43 V7) for 1998 to 2018 (ref. 67) and (2) monthly precipitation (0.5° resolution) from the Global Precipitation Climatology Centre (GPCC, Version 7) database for 1970 to 1998 (ref. 68). The GPCC dataset was regridded to match the resolution of TRMM. TRMM and GPCC were then regressed for the overlapping time period (1998–2003, that is, January TRMM versus January GPCC) for all neotropical forest pixels, and the fit is used to correct the GPCC data to match TRMM. The 1970–2018 precipitation record (P) includes monthly adjusted GPCC data (1970–1998) and monthly TRMM data from 1998 to 2018.

Again, for a finer spatial resolution we downscaled precipitation data for plot locations followed a procedure similar to that used for temperature: upscaling to 1 km² resolution using WorldClim (v2 (ref. 66)). The GPCC–TRMM precipitation record is resampled to match the resolution of WorldClim, and the mean (μ) GPCC–TRMM precipitation for the period 1970–2000 is calculated for each month. The monthly ratio ($P_{\text{ratio}} = P_{\mu}/P_{\text{WorldClim}}$) of the mean climate is calculated, and P_{ratio} used to adjust monthly precipitation 1970–2017: $P_{\text{plot}} = P \times P_{\text{ratio}}$.

The drought intensity experienced by plots was estimated as the MCWD. The MCWD was calculated as in ref. 69 and accounts for plot seasonality as calculations take place for each pixel:

$$\text{if } WD_{n-1} - ET_n + P_n < 0;$$

$$\text{then } WD_n = WD_{n-1} - ET_n + P_n;$$

$$\text{else } WD_n = 0.$$

where WD is water deficit, n indicates month, ET is evapotranspiration and P is precipitation.

We assumed a constant monthly evapotranspiration of 100 mm per month based on measurements from Amazonia^{69,70} and as used in previous studies^{8,10}. This is similar to an estimate of variable ET we calculated for the 123 plots based on monthly precipitation and temperature, *sensu*⁷¹, a mean ET value of 102 mm per month. This allows MCWD to represent a precipitation-driven dry season deficit, meaning that MCWD is temperature independent, allowing us to discriminate between temperature- and drought-driven changes in growth and mortality.

We used census dates to calculate climate anomalies for each plot. For the pre-El Niño monitoring period of a plot we calculate the mean of the annual MCWD values, that is, the pre-El Niño drought state. For the 2015–2016 El Niño census interval we select the maximum annual MCWD value, as we are interested in the most extreme drought conditions within the El Niño sampling window for each plot. We used the 12 month period from May 2015 to April 2016, the 12 consecutive months with the greatest sea surface temperature anomalies in the Niño 3.4 region³⁵, for visualizing El Niño climate anomalies and pre-El Niño climate.

Reporting summary

Further information on research design is available in the Nature Portfolio Reporting Summary linked to this article.

Data availability

Publicly available climate data used in this paper are available from ERA5 (ref. 64), CRU ts.4.03 (ref. 65), WorldClim v2 (ref. 66), TRMM product 3B43 V7 (ref. 67) and GPCC, Version 7 (ref. 68). The input data are available on ForestPlots⁴².

Code availability

R code for graphics and analyses is available on ForestPlots⁴².

References

39. Pezzini, F. et al. The Brazilian Program for Biodiversity Research (PPBio) Information System. *Biodivers. Ecol.* **4**, 265–274 (2012).
40. Malhi, Y. et al. An international network to monitor the structure, composition and dynamics of Amazonian forests (RAINFOR). *J. Veg. Sci.* **13**, 439–450 (2002).
41. ForestPlots.net et al. Taking the pulse of Earth's tropical forests using networks of highly distributed plots. *Biol. Conserv.* <https://doi.org/10.1016/j.biocon.2020.108849> (2021).
42. Bennett, A. C. et al. Data package for 'Sensitivity of South American tropical forests to an extreme climate anomaly'. *ForestPlots.NET* https://doi.org/10.5521/forestplots.net/2023_2 (2023).
43. Phillips, O. et al. RAINFOR field manual for plot establishment and remeasurement. In *R Soc 1*–22 (2016).
44. Qie, L. et al. Long-term carbon sink in Borneo's forests halted by drought and vulnerable to edge effects. *Nat. Commun.* **8**, 1966 (2017).
45. Sullivan, M. J. P. et al. Long-term thermal sensitivity of Earth's tropical forests. *Science* **368**, 869–874 (2020).
46. Talbot, J. et al. Methods to estimate aboveground wood productivity from long-term forest inventory plots. *For. Ecol. Manag.* **320**, 30–38 (2014).
47. Lewis, S. L. et al. Increasing carbon storage in intact African tropical forests. *Nature* **457**, 1003–1006 (2009).
48. Lewis, S. L. et al. Above-ground biomass and structure of 260 African tropical forests. *Philos. Trans. R. Soc. B* **368**, 20120295 (2013).
49. Chave, J. et al. Improved allometric models to estimate the aboveground biomass of tropical trees. *Glob. Change Biol.* **20**, 3177–3190 (2014).
50. Goodman, R. C. et al. Amazon palm biomass and allometry. *For. Ecol. Manage.* **310**, 994–1004 (2013).
51. Zanne, A. E. et al. Data from: towards a worldwide wood economics spectrum. *Dryad* <https://doi.org/10.5061/DRYAD.234> (2009).
52. Chave, J. et al. Towards a worldwide wood economics spectrum. *Ecol. Lett.* **12**, 351–366 (2009).
53. Lopez-Gonzalez, G., Lewis, S. L., Burkitt, M. & Phillips, O. L. ForestPlots.net: a web application and research tool to manage and analyse tropical forest plot data: ForestPlots.net. *J. Veg. Sci.* **22**, 610–613 (2011).
54. Sullivan, M. J. P. et al. Field methods for sampling tree height for tropical forest biomass estimation. *Methods Ecol. Evol.* **9**, 1179–1189 (2018).
55. López-Gonzalez, G., Sullivan, M. J. P. & Baker, T. R. BiomasaFP: tools for analysing data downloaded from ForestPlots.net. R package version 0.3.0. (2015).
56. Martin, A. R., Doraisami, M. & Thomas, S. C. Global patterns in wood carbon concentration across the world's trees and forests. *Nat. Geosci.* **11**, 915–920 (2018).
57. Lewis, S. L. et al. Tropical forest tree mortality, recruitment and turnover rates: calculation, interpretation and comparison when census intervals vary. *J. Ecol.* **92**, 929–944 (2004).
58. Kloeke, J. D. & McKean, J. W. Rfit: rank-based estimation for linear models. *R. J.* **4**, 57 (2012).
59. Dormann, C. F. et al. Collinearity: a review of methods to deal with it and a simulation study evaluating their performance. *Ecography* **36**, 27–46 (2013).
60. Sheather, S. J. *A Modern Approach to Regression with R* (Springer, 2009).
61. Bates, D. et al. lme4: linear mixed-effects models using 'Eigen' and S4. R Project <https://CRAN.R-project.org/package=lme4> (2022).
62. Symonds, M. R. E. & Moussalli, A. A brief guide to model selection, multimodel inference and model averaging in behavioural ecology using Akaike's information criterion. *Behav. Ecol. Sociobiol.* **65**, 13–21 (2011).
63. Barton, K. MuMIn: multi-model inference. R package version 1.46.5. <https://CRAN.R-project.org/package=MuMIn> (2022).
64. Copernicus Climate Change Service (C3S). ERA5: Fifth Generation of ECMWF Atmospheric Reanalyses of the Global Climate (Copernicus Climate Change Service Climate Data Store, 2017).
65. University of East Anglia Climatic Research Unit, Harris, I. C. & Jones, P. D. CRU TS4.03: Climatic Research Unit (CRU) Time-Series (TS) Version 4.03 of High-Resolution Gridded Data of Month-by-Month Variation in Climate (Jan. 1901–Dec. 2018) (Centre for Environmental Data Analysis, 2020).
66. Fick, S. E. & Hijmans, R. J. WorldClim 2: new 1-km spatial resolution climate surfaces for global land areas. *Int. J. Climatol.* **37**, 4302–4315 (2017).
67. Huffman, G. J. et al. The TRMM Multisatellite Precipitation Analysis (TMPA): quasi-global, multiyear, combined-sensor precipitation estimates at fine scales. *J. Hydrometeorol.* **8**, 38–55 (2007).
68. Schneider, U. et al. GPCP full data reanalysis version 6.0 at 0.5°: monthly land-surface precipitation from rain-gauges built on GTS-based and historic data: gridded monthly totals. 20–270 MB per decadal gzip compressed NetCDF archive. Federal Ministry of Transport and Digital Infrastructure https://doi.org/10.5676/DWD_GPCP/FD_M_V6_050 (2011).
69. Aragão, L. E. O. C. et al. Spatial patterns and fire response of recent Amazonian droughts. *Geophys. Res. Lett.* **34**, L07701 (2007).
70. Aragão, L. E. O. C. et al. Environmental change and the carbon balance of Amazonian forests: environmental change in Amazonia. *Biol. Rev.* **89**, 913–931 (2014).
71. Hamon, W. R. Computation of direct runoff amounts from storm rainfall. *Int. Assoc. Sci. Hydrol. Publ.* **63**, 63 (1963).

Acknowledgements

This paper is a product of the Amazon Forest Inventory Network (RAINFOR) and the Programa de Pesquisa em Biodiversidade (PPBio), and their combined plot data curated at ForestPlots.net. We gratefully acknowledge field assistants who contributed to the El Niño remeasurement campaigns: D. Aguilar Flores, L. Alfaro Curitumay, K. Alves Cavaleiro, W. Alves da Cruz, E. Alves Hernandez, G. Aramayo, J. Araújo de Souza, J. Ataliba Mantelli Aboim Gomes, M. Baisie, E. Ballesteros Miguel, J. Betancourt, M. Betancur Nuñez, E. Borges Brito, A. Cardoso, J. Manuel Castro, J. Carlos Chore Egues, E. Ignacio Sebastian Ciriaco, A. Cuevas, J. da Costa Freitas, D. da Cruz Viana, M. da Silva Melo, B. de Oliveira, T. de Souza Valente Júnior, J. Carlos Dib, D. do Nascimento Reis Junior, J. Engel, W. Farfan-Rios, J. Raimundo Ferreira Nunes, F. França, L. Enrique Gámez, I. Garcia Ferreira, R. Garcia Paz-Soldan, S. Gonçalves Longhi, T. Dario Gutierrez, G. Hidalgo Pizango, G. Huari Jimenez, L. Jordan Gallegos, N. Kapashi Ahuanari, M. Kapeshi Ahyani, M. Koese, F. Kwasie, R. Ledezma Vargas, S. Lopes Pinheiro, C. Heloísa Luz de Oliveira, F. Martinez Achacollo, M. Martinez Ugarteche, L. Meireles, D. Mendes Santos, C. Mendoza, J. Mucherino, R. Nina, Angélica Oliveira Müller, P. Naisso, O. Ngwete, R. Carlos Paca Condori, P. Pascal, A. Peña Cruz, P. Petronelli, F. Prado Assunção, E. Queiroz Marques, A. Manuel Ramos Peña, J. Reyna Huaymacari, N. G. Ribeiro Júnior, J. Rodríguez Pacaya, F. Rojas, R. Rojas Gonzales, M. Elena Rojas Peña, N. A. Rosa, C. Roth, P. Salcedo, R. Sante, M. Seixas, G. Shareva Mateo, A. Silva Lima, D. Silva Nogueira, H. Vásquez Vásquez, D. Villarroel, L. James Yansen, S. Abzalón Zamora López and R. Zehnder Torres. For their important contributions to developing RAINFOR and its antecedents we are indebted to J. Lloyd and our late colleagues, E. Armas, T. Erwin, A. Gentry, S. Patiño and J.-P. Veillon. We highlight the principal investigators and grants that funded the El Niño

remeasurement campaigns: remeasurements in Peru were funded by Gordon and Betty Moore Foundation (grant number 5349; 'MonANPeru: Monitoring Protected Areas in Peru to Increase Forest Resilience to Climate Change'), a Royal Society Global Challenges grant (Sensitivity of Tropical Forest Ecosystem Services to Climate Changes) funded the censuses in Colombia and Minas Gerais, CNPq grants (441282/2016-4, 403764/2012-2 and 558244/2009-2) funded the central Amazon Long-Term Ecological Project, FAPEAM grants 1600/2006, 465/2010 and PPFOR 147/2015 funded the PPBio plots in the central Amazon, and CNPq grants 473308/2009-6 and 558320/2009-0 funded the monitoring of Purus-Madeira interfluvium. RAINFOR, PPBio and ForestPlots.net have been supported by numerous people and grants since their inception. For supporting the networks, we thank the European Research Council (ERC Advanced Grant 291585—'T-FORCES'), the Gordon and Betty Moore Foundation (#1656 'RAINFOR', and 'MonANPeru'), the European Union's Fifth, Sixth and Seventh Framework Programme (EVK2-CT-1999-00023—'CARBONSINK-LBA', 283080—'GEOCARBON', and 282664—'AMAZALERT'), the Natural Environment Research Council (NE/ D005590/1—'TROBIT', NE/FO05806/1—'AMAZONICA', and E/M0022021/1—'PPFOR'), several NERC Urgency and New Investigators Grants, the NERC/State of São Paulo Research Foundation (FAPESP) consortium grants 'BIO-RED' (NE/NO12542/1), 'ECOFOR' (NE/KO16431/1, FAPESP 2012/51872-5 and 2012/51509-8), 'ARBOLES' (NE/SO11811/1 and FAPESP 2018/15001-6), 'SEOSAW' (NE/PO08755/1), 'SECO' (NE/TO1279X/1), Brazilian National Research Council (PELD/CNPq 403710/2012-0), the Royal Society (University Research Fellowships and Global challenges Awards) (ICA/R1/180100—'FORAMA'), the National Geographic Society, US National Science Foundation (DEB 1754647) and Colombia's Colciencias. We thank the National Council for Science and Technology Development of Brazil (CNPq) for support to the Cerrado/Amazonia Transition Long-Term Ecology Project (PELD/441244/2016-5), the PPBio Phytogeography of Amazonia/Cerrado Transition Project (CNPq/PPBio/457602/2012-0), PELD-RAS (CNPq, Process 441659/2016-0), RESFLORA (Process 420254/2018-8), Synergize (Process 442354/2019-3), the Empresa Brasileira de Pesquisa Agropecuária—Embrapa (SEG: 02.08.06.005.00), the Fundação de Amparo à Pesquisa do Estado de São Paulo—FAPESP BIOTA (2012/51509-8 and 2012/51872-5), the Goiás Research Foundation (FAPEG/PELD: 2017/10267000329) the EcoSpace Project (CNPq 459941/2014-3) and several PVE and Productivity Grants. We also thank the 'Investissement d'Avenir' programme (CEBA, ref. ANR-10LABX-25-01), the São Paulo Research Foundation (FAPESP 03/12595-7) and the Sustainable Landscapes Brazil Project (through Brazilian Agricultural Research Corporation (EMBRAPA), the US Forest Service, USAID, and the US Department of State) for supporting plot inventories in the Atlantic Forest sites in São Paulo, Brazil. Further funding sources include CNPq (processes 305054/2016-3 and 442371/2019-5) to L.E.O.C.A., a NERC Knowledge Exchange Fellowship (NE/VO18760/1) to E.N.H.C., the Coordenação de Aperfeiçoamento de Pessoal de Nível Superior—Brasil (CAPES)—Finance Code 001 to T.E. We thank the National Council for Technological and Scientific Development (CNPq) for the financial support of the PELD project (441244/2016-5, 441572/2020-0) and FAPEMAT (0346321/2021). This manuscript is an output of

ForestPlots.net Research Project 36, 'Impact of the 2015/2016 El Niño on South American tropical forests'. ForestPlots.net is a meta-network and cyber-initiative developed at the University of Leeds that unites permanent plot records and supports scientists working in the world's tropical forests. We acknowledge the contributions of the ForestPlots.net Collaboration and Data Request Committee (B.S.M., E.N.H.C., O.L.P., T.R.B., B. Sonké, C. Ewango, J. Muledi, S.L.L. and L. Qie) for facilitating this project and associated data management. The development of ForestPlots.net and curation of data has been funded by several grants including NE/B503384/1, NE/NO12542/1—'BIO-RED', ERC Advanced Grant 291585—'T-FORCES', NE/FO05806/1—'AMAZONICA', NE/NO04655/1—'TREMOR', NERC New Investigators Awards, the Gordon and Betty Moore Foundation ('RAINFOR', 'MonANPeru'), ERC Starter Grant 758873—'TreeMort', EU Framework 6, a Royal Society University Research Fellowship, and a Leverhulme Trust Research Fellowship. For supporting A.C.B. we thank the European Space Agency ('ForestScan' 4000126857/20/NL/AI), NERC ('ARBOLES' (NE/SO11811/1, FAPESP 2018/15001-6)), the Royal Society (Global Challenges Award, ICA/R1/180100—'FORAMA') and a University of Leeds NERC Doctoral Training Partnership studentship (NE/LO02574/1).

Author contributions

A.C.B., S.L.L. and O.L.P. designed research; all authors performed research, contributed data and had the chance to comment on the manuscript; M.J.P.S., A.L. and G.C.P. contributed new analytic tools; O.L.P. managed the forest plot remeasurement programme; A.C.B. analysed data; and A.C.B. and O.L.P. wrote the paper with input from all authors. El Niño remeasurement campaigns were led by T.R.S., A.M.-M., A.E.-M., P.S.M., F.C.S., W.C., L.F.D., G.F.L., R.M.S., E.R., E.V.T., E.A.-D., T.R.B., F.R.C.C., B.S.M., J.S., B.B., E.B., A.A.-M., Z.R.C., W.L., F.D.S., L.J.V., F.E., R.V.M., B.H.M.-J., D.G., M.J.P.S., J.B., L.F.A., S.A.V., L.A., D.B., G.D., M.D., M.S., A.D., T.F., J.F., V.F.M., G.G.S., B.H., E.H.C., C.J., F.A.M.S., Y.M., H.R.A., G.S., M.S., Y.S.S., L.V.G. and O.L.P.

Competing interests

The authors declare no competing interests.

Additional information

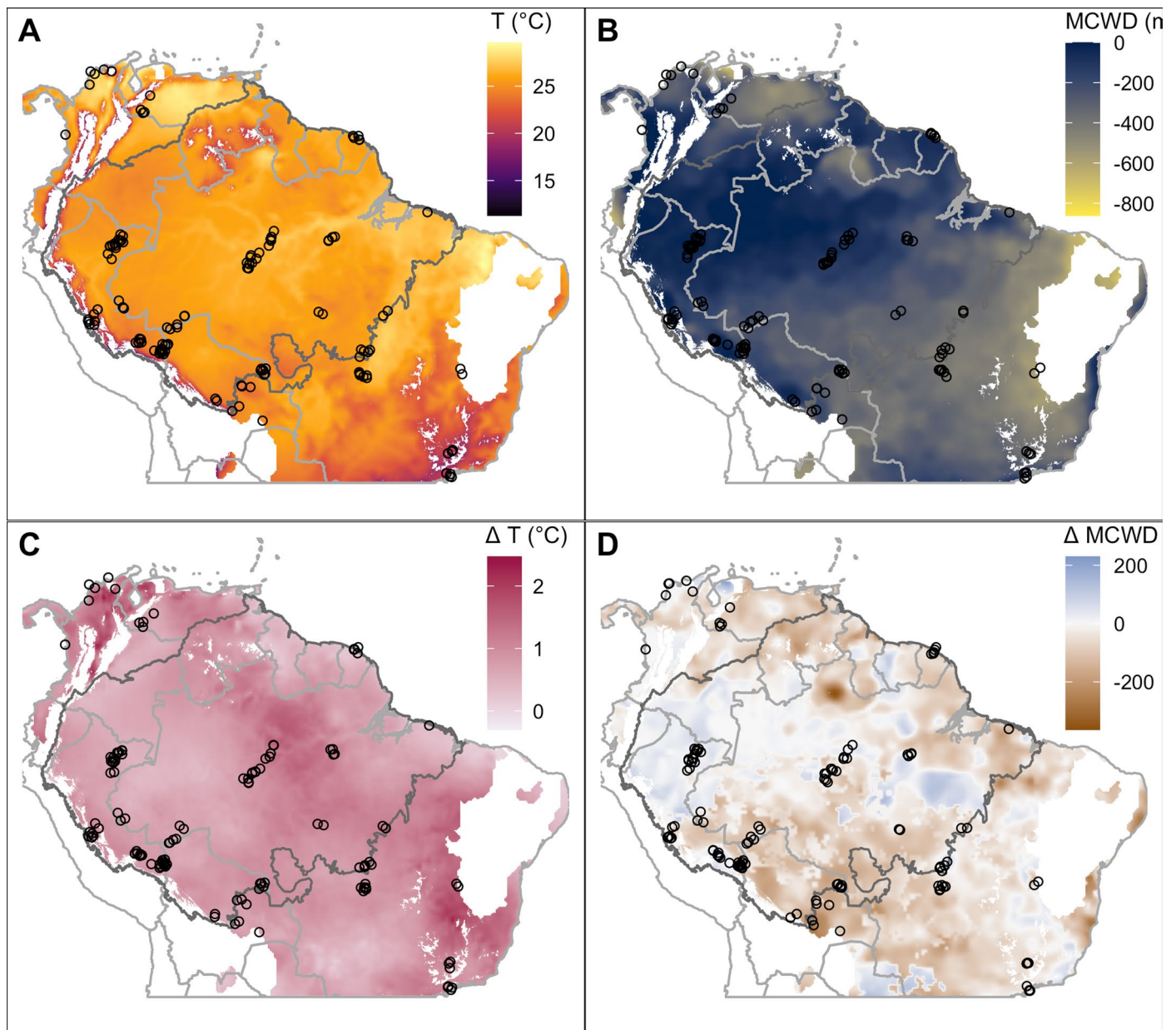
Extended data is available for this paper at <https://doi.org/10.1038/s41558-023-01776-4>.

Supplementary information The online version contains supplementary material available at <https://doi.org/10.1038/s41558-023-01776-4>.

Correspondence and requests for materials should be addressed to Amy C. Bennett.

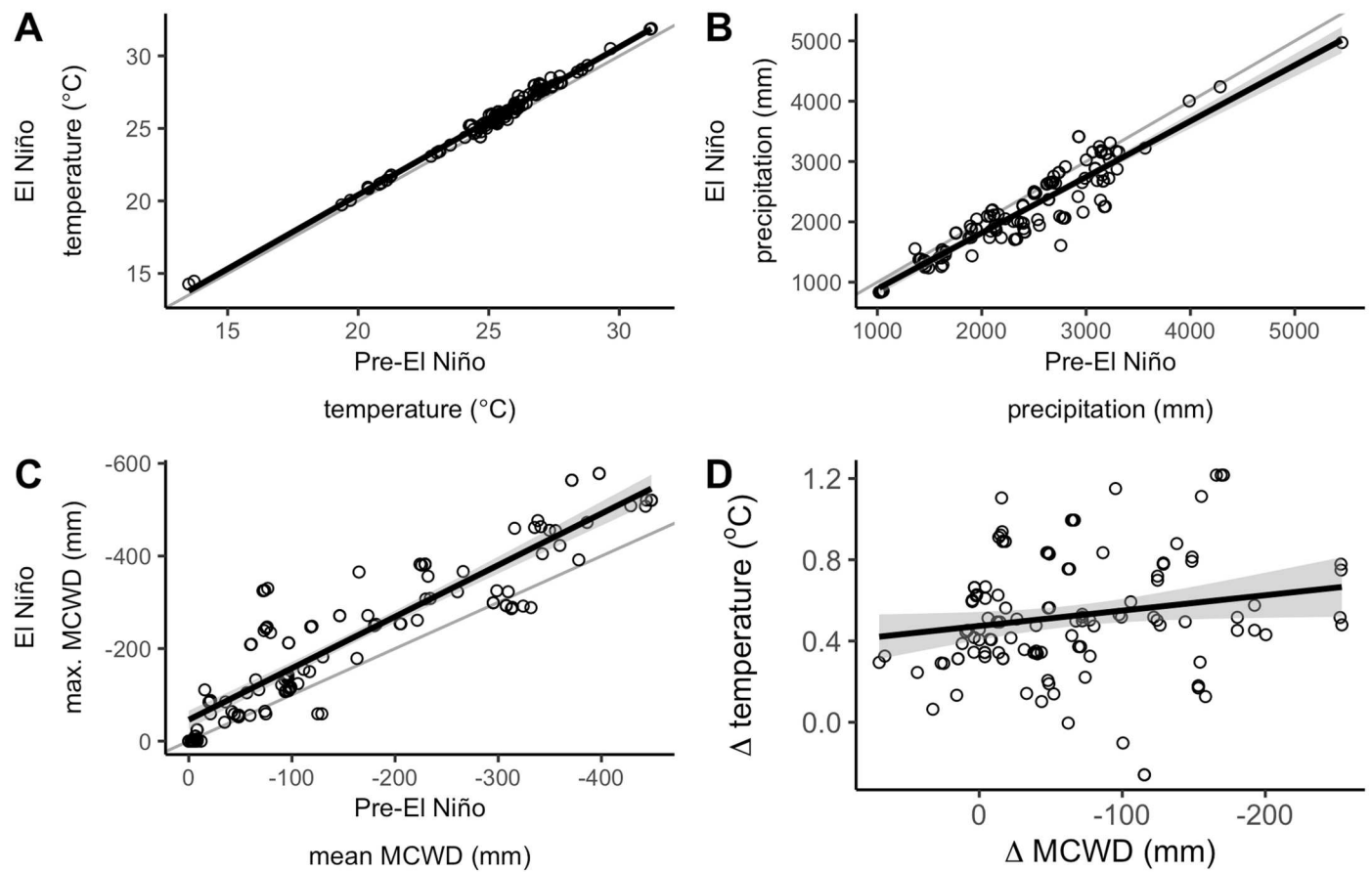
Peer review information *Nature Climate Change* thanks Akira Mori, César Terrer and the other, anonymous, reviewer(s) for their contribution to the peer review of this work.

Reprints and permissions information is available at www.nature.com/reprints.



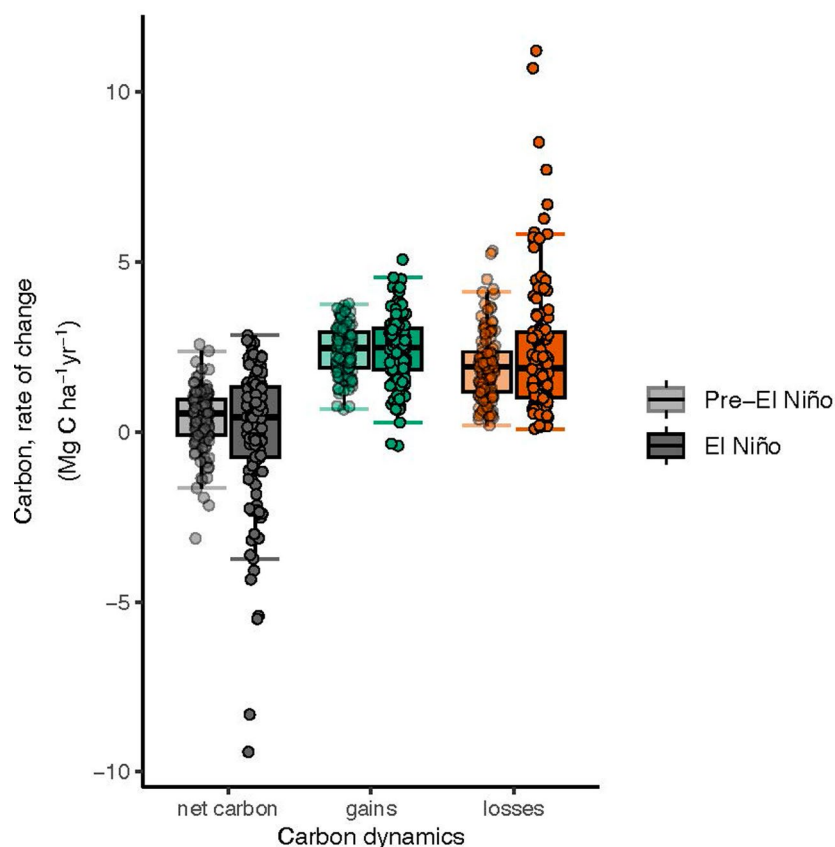
Extended Data Fig. 1 | Pre-El Niño climate and 2015–2016 El Niño climate anomalies and locations of 123 forest plots. Pre-El Niño temperature (a), pre-El Niño drought (b), temperature anomaly (c) and drought anomaly (d) and locations of forest plots (black circles). Pre-El Niño temperature, T , is the average mean monthly temperature May 2005–April 2015 (A). Pre-El Niño maximum cumulative water deficit, MCWD (mm), is the mean MCWD May 2005–April

2015 (B). The intensity of temperature change, ΔT , is the average mean monthly temperature in the El Niño year minus the average of the preceding decade (C). The intensity of MCWD change, ΔMCWD , is the MCWD in the El Niño year minus the average of the preceding decade (D). The Amazon basin is delineated by a dark grey line. Plot locations are indicated by black circles which can overlap.



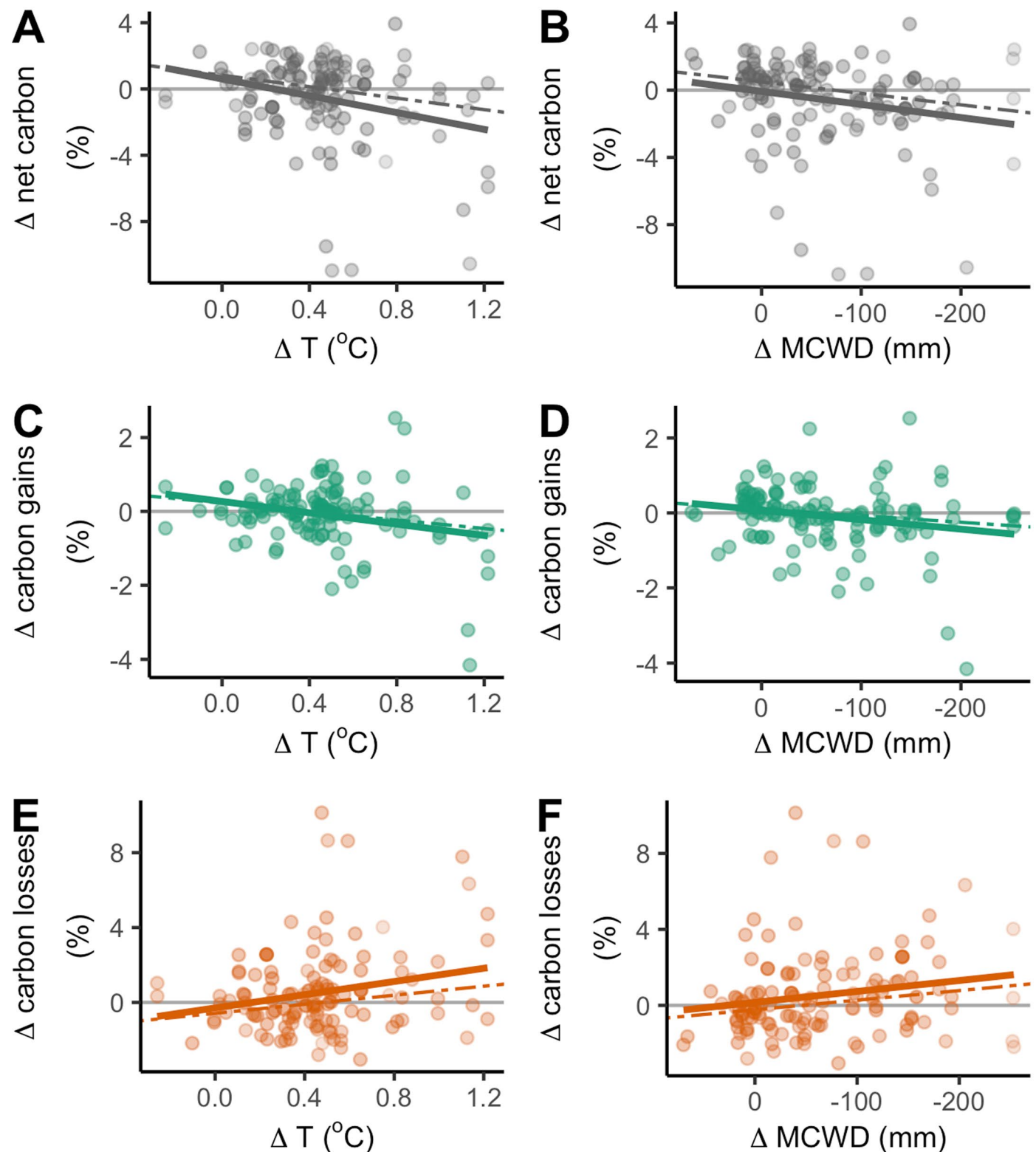
Extended Data Fig. 2 | Climate anomalies of 123 long-term inventory plots. Pre-El Niño and El Niño are defined by plot census dates. Plot census interval pre-El Niño and El Niño temperature (a), linear model $p < 0.0001$, annual precipitation (b), $p < 0.0001$, maximum cumulative water deficit MCWD

(c), $p < 0.0001$, and change in maximum cumulative water deficit MCWD and temperature (d), $p = 0.008$, in plots. $n = 123$ plots censused pre- and El Niño. Grey line indicates 1:1 relationship, grey shading indicates standard error.



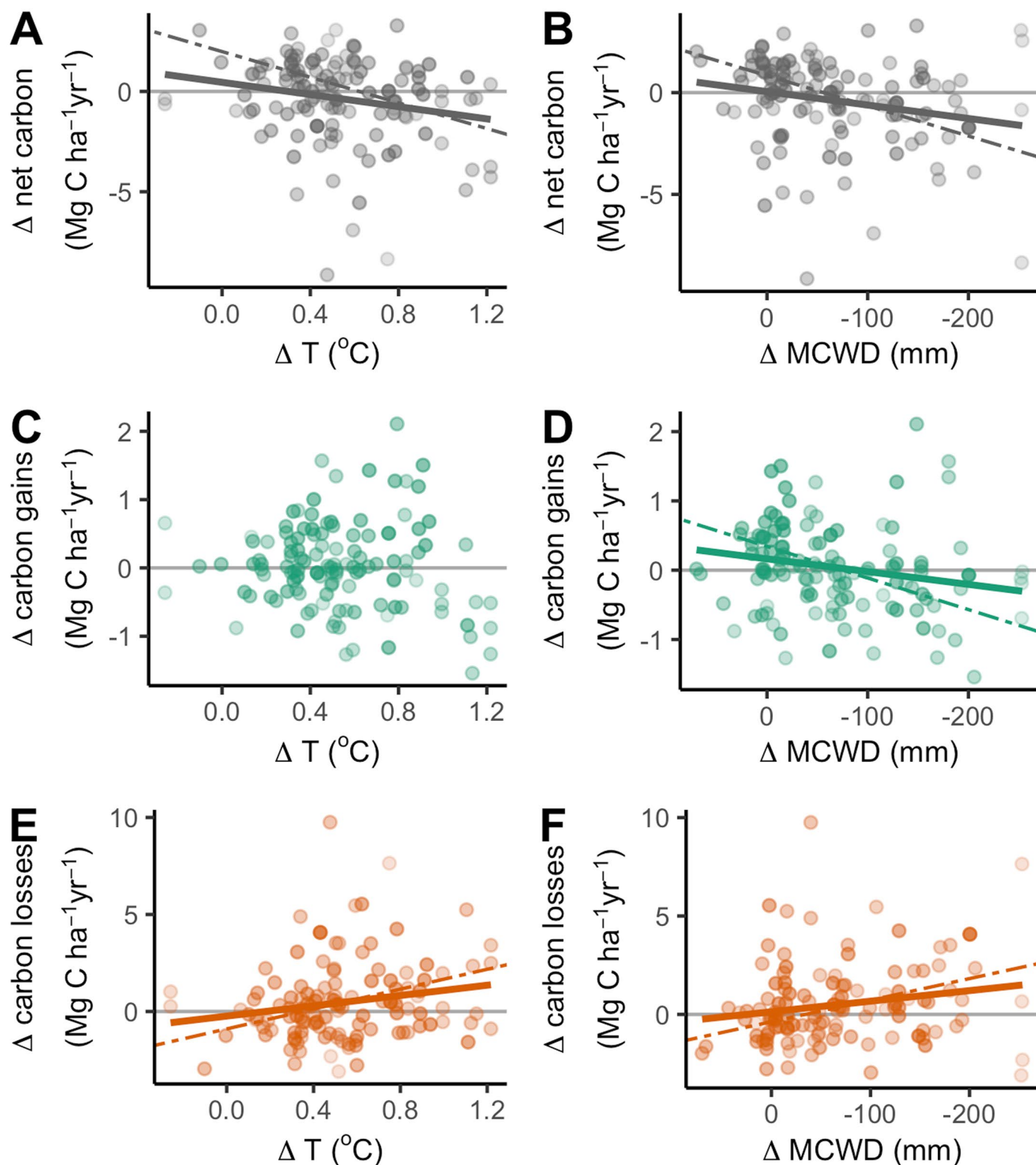
Extended Data Fig. 3 | Boxplots of aboveground carbon changes and in 123 forest plots during the 2015–2016 El Niño event. Corresponding to Fig. 1d in the main text, points show plot-level information, $n = 123$ plots, horizontal black

line indicates median, the lower and upper hinges are the first and third quartiles, the whiskers extend to the value furthest from the hinge but no more than $1.5 \times$ interquartile range.



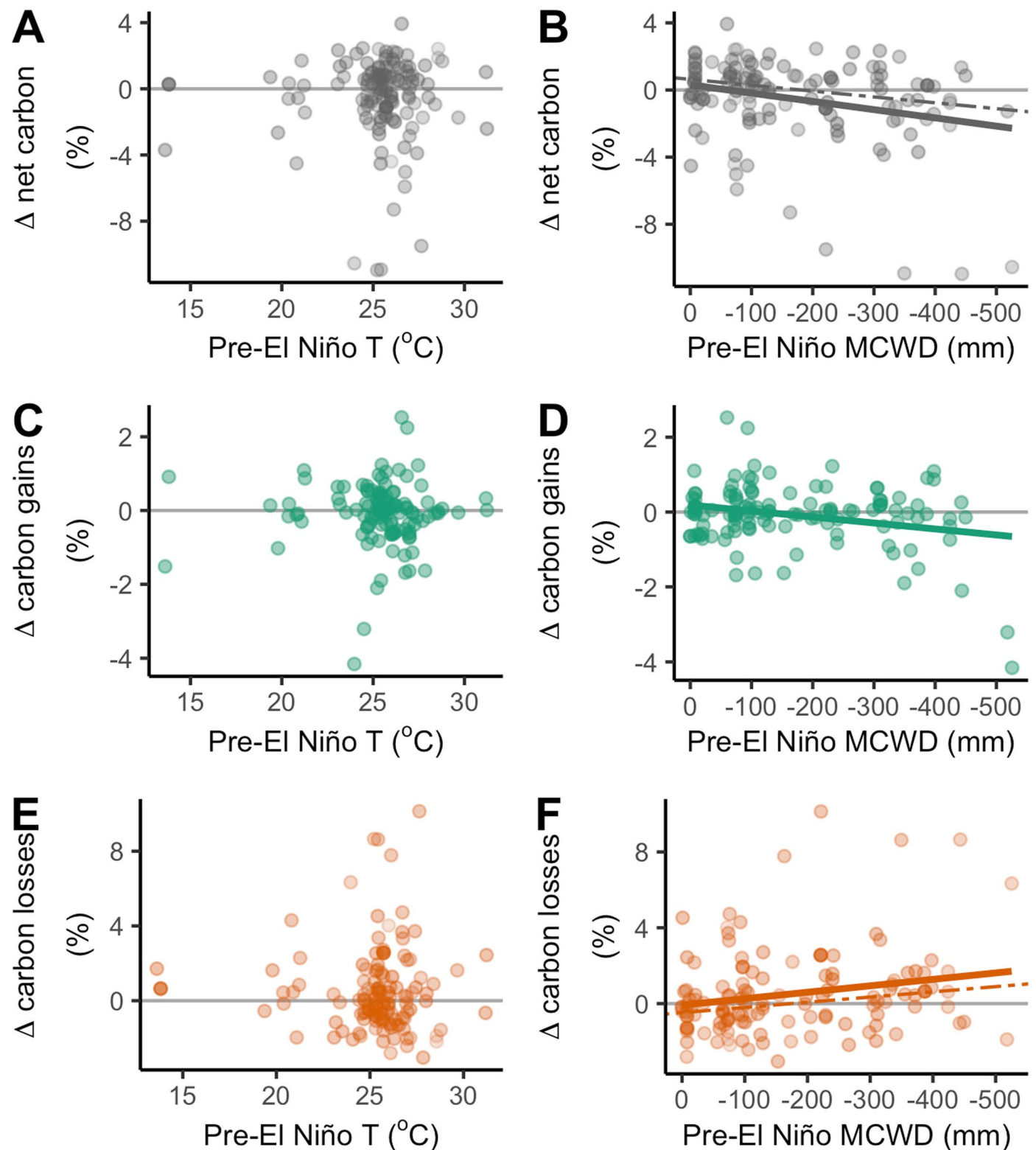
Extended Data Fig. 4 | Effects of the 2015–2016 El Niño climate anomaly on aboveground biomass carbon dynamics in 123 neotropical forest plots, for forests measured after 2000. Temperature anomaly (left) and drought anomaly (right) impacts on aboveground biomass carbon dynamics as relative change. The net carbon change (a, b), carbon gains from recruitment and growth (c, d) and carbon losses from mortality (e, f) of the censuses capturing the El Niño event minus pre-El Niño plot monitoring period for 123 long-term inventory plots. The temperature change, Δ temperature (T) (A, C, E) is mean monthly temperature in the El Niño census interval minus mean monthly temperature pre-El Niño, using the census dates of the plot censuses. The intensity of the change in dry season strength, is calculated as Δ maximum cumulative water deficit (MCWD) (B, D, F)

which is the difference between maximum MCWD in El Niño and mean MCWD in pre-El Niño. Point shading from light to dark denotes greater weighting, with plots and line of best fit weighted by an empirically derived combination of pre-El Niño plot monitoring length and plot area for each response variable. Solid lines indicate significant linear models ($p < 0.05$) and dashed lines represent significant one-tailed Kendall's Tau correlation tests using rank-based linear model estimation ($p < 0.05$). Slopes, intercepts and p-values for significant linear models are as follows: A: $y = -2.5x + 0.6$, $p = 0.002$; B: $y = -0.008x - 0.08$, $p = 0.02$; C: $y = -0.8x + 0.3$, $p = 0.003$; D: $y = -0.003x + 0.08$, $p = 0.02$; E: $y = 1.8x - 0.3$, $p = 0.01$; F: $y = 0.006x + 0.2$, $p = 0.048$.



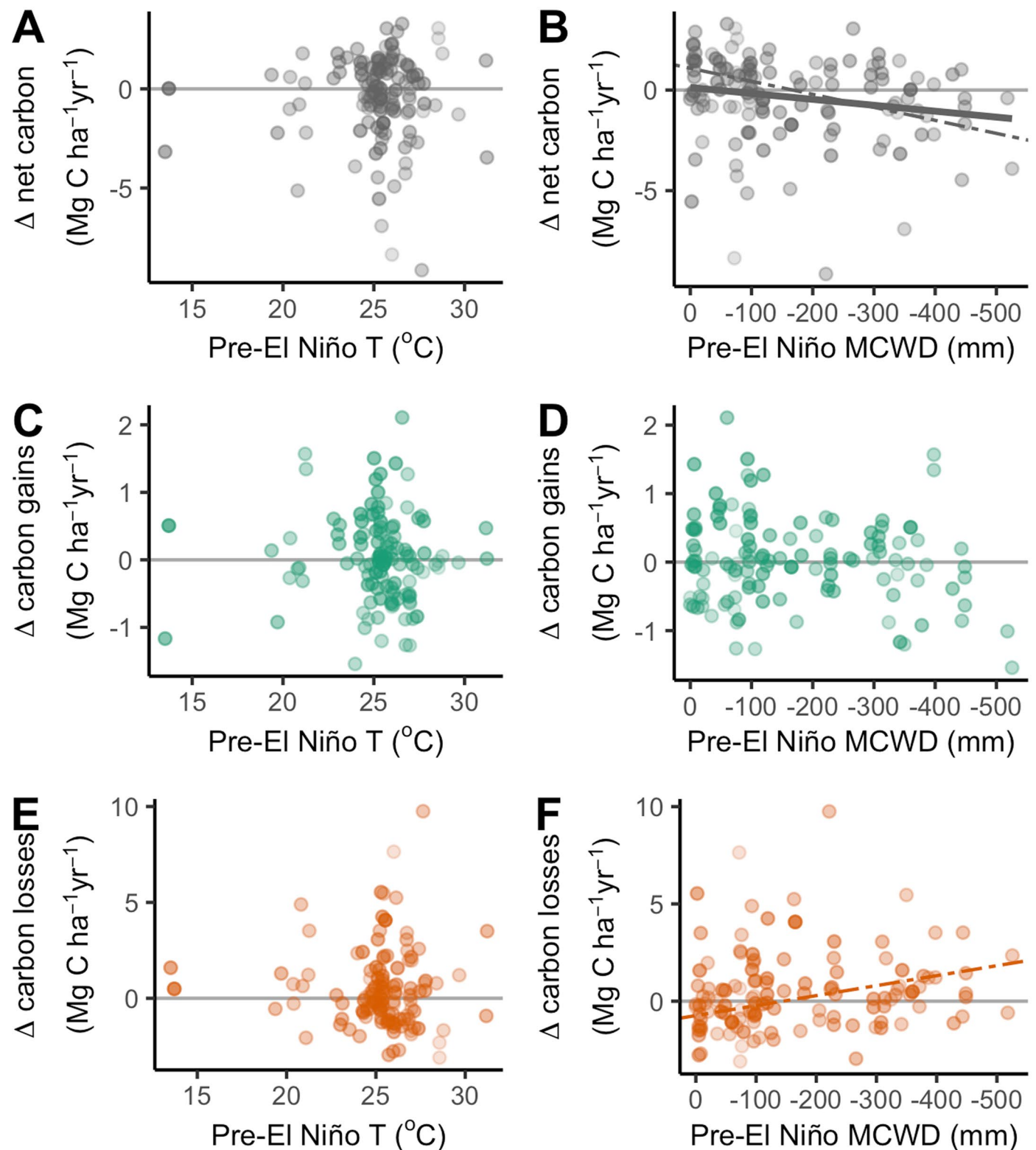
Extended Data Fig. 5 | Effects of the 2015–2016 El Niño climate anomaly on aboveground biomass carbon dynamics in 123 neotropical forest plots, with carbon changes expressed in absolute terms. Temperature anomaly (left) and drought anomaly (right) impacts on aboveground biomass carbon dynamics as absolute change. The net carbon change (**a, b**), carbon gains from recruitment and growth (**c, d**) and carbon losses from mortality (**e, f**) of the censuses capturing the El Niño event minus pre-El Niño plot monitoring period for 123 long-term inventory plots. The temperature change, Δ temperature (T) (**A, C, E**) is mean monthly temperature in the El Niño census interval minus mean monthly temperature pre-El Niño, using the census dates of the plot censuses. The intensity of the change in dry season strength, is calculated as Δ maximum

cumulative water deficit (MCWD) (**B, D, F**) which is the difference between maximum MCWD in El Niño and mean MCWD in pre-El Niño. Point shading from light to dark denotes greater weighting, with plots and line of best fit weighted by an empirically derived combination of pre-El Niño plot monitoring length and plot area for each response variable. Solid lines indicate significant linear models ($p < 0.05$) and dashed lines represent significant one-tailed Kendall's Tau correlation tests using rank-based linear model estimation ($p < 0.05$). Slopes, intercepts and p -values for significant linear models are as follows: **A**: $y = -3.3x + 1$, $p = 0.02$; **B**: $y = -0.01x + 0.1$, $p = 0.01$; **D**: $y = -0.004x + 0.4$, $p = 0.02$; **E**: $y = 2.9x - 0.5$, $p = 0.03$; **F**: $y = 0.01x + 0.3$, $p = 0.04$.



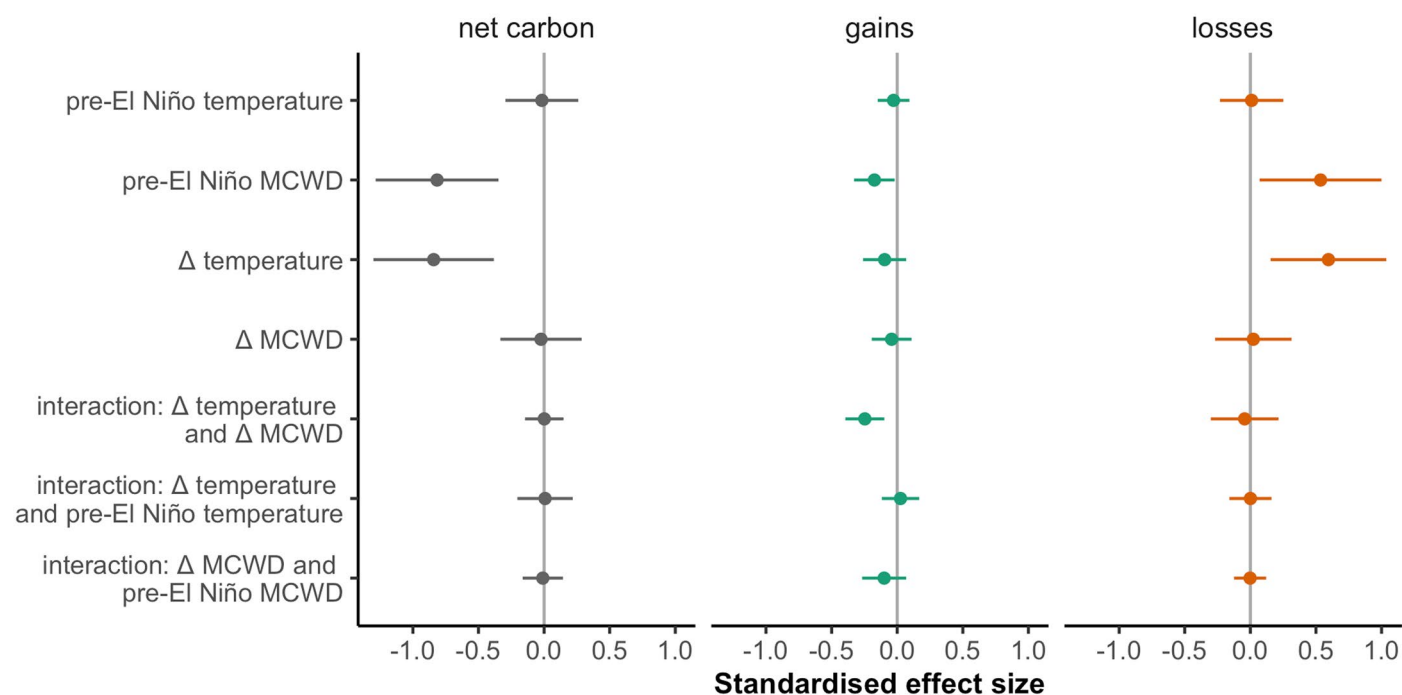
Extended Data Fig. 6 | Effects of the 2015–2016 El Niño climate anomaly on aboveground biomass carbon dynamics in 123 neotropical forest plots, for forests measured after 2000. Pre-El Niño temperature (left) and pre-El Niño drought (right) impacts on aboveground biomass carbon dynamics as relative change. The net carbon change (**a**, **b**), carbon gains from recruitment and growth (**c**, **d**) and carbon losses from mortality (**e**, **f**) of the censuses capturing the El Niño event minus pre-El Niño plot monitoring period for 123 long-term inventory plots. The pre-El Niño temperature (T) (**A**, **C**, **E**) is the mean of mean monthly temperature in the monitoring period prior to the El Niño, using the census dates of the plot censuses. The pre-El Niño maximum cumulative water deficit

(MCWD) (**B**, **D**, **F**) is the mean MCWD in the monitoring period prior to the El Niño. Point shading from light to dark denotes greater weighting, with plots and line of best fit weighted by an empirically derived combination of pre-El Niño plot monitoring length and plot area for each response variable. Solid lines indicate significant linear models ($p < 0.05$) and dashed lines represent significant one-tailed Kendall's Tau correlation tests using rank-based linear model estimation ($p < 0.05$). Slopes, intercepts and p -values for significant linear models are as follows: **B**: $y = -0.005x + 0.3$, $p = 0.003$; **D**: $y = -0.002x + 0.2$, $p = 0.003$; **E**: $y = 0.003x - 0.08$, $p = 0.02$.



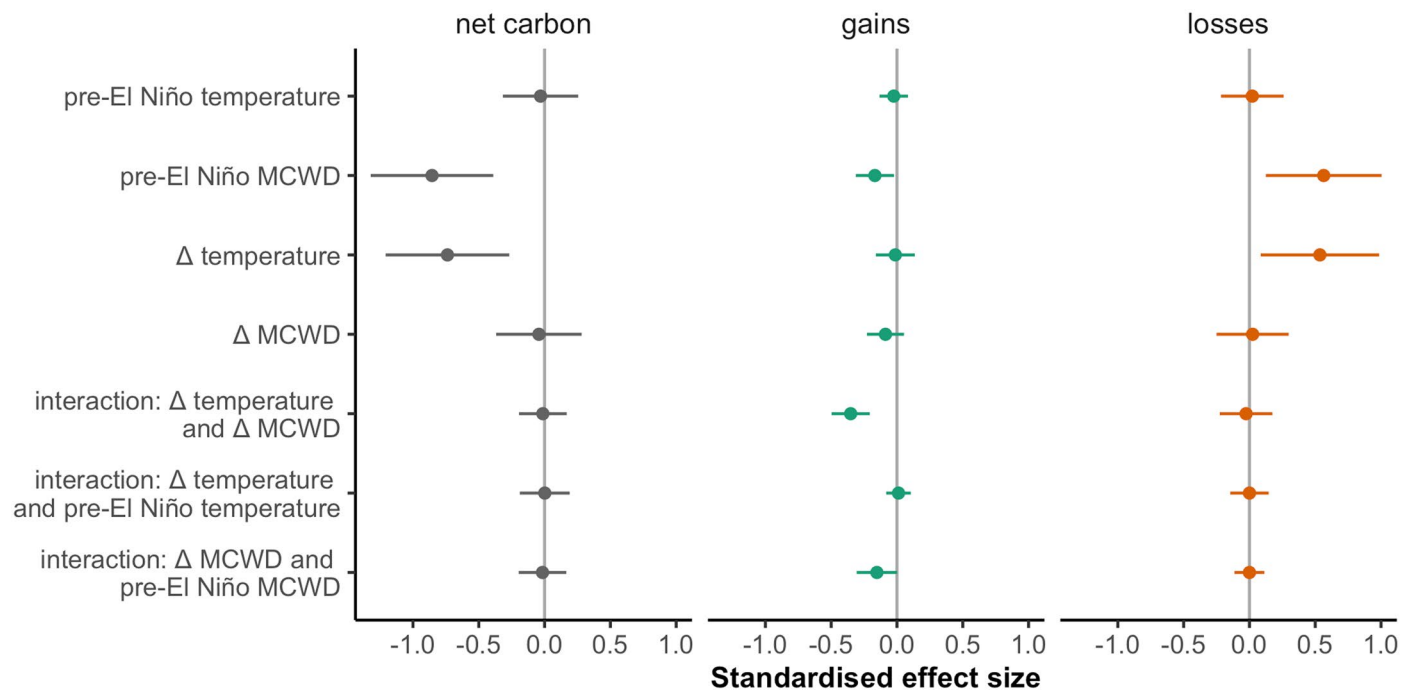
Extended Data Fig. 7 | Effects of the 2015–2016 El Niño climate anomaly on aboveground biomass carbon dynamics in 123 neotropical forest plots, with carbon changes expressed in absolute terms. Pre-El Niño temperature (left) and pre-El Niño drought (right) impacts on aboveground biomass carbon dynamics as absolute change. The net carbon change (a, b), carbon gains from recruitment and growth (c, d) and carbon losses from mortality (e, f) of the censuses capturing the El Niño event minus pre-El Niño plot monitoring period for 123 long-term inventory plots. The pre-El Niño temperature (T) (A, C, E) is the mean of mean monthly temperature in the monitoring period prior to the El Niño, using the census dates of the plot censuses. The pre-El Niño maximum

cumulative water deficit (MCWD) (B, D, F) is the mean MCWD in the monitoring period prior to the El Niño. Point shading from light to dark denotes greater weighting, with plots and line of best fit weighted by an empirically derived combination of pre-El Niño plot monitoring length and plot area for each response variable. Solid lines indicate significant linear models ($p < 0.05$) and dashed lines represent significant one-tailed Kendall's Tau correlation tests using rank-based linear model estimation ($p < 0.05$). Slopes, intercepts and p-values for significant linear models are as follows: B: $y = -0.006x + 0.3$, $p = 0.03$; F: linear model is not significant, $p = 0.1$, but rank-based model is, $p = 0.007$.



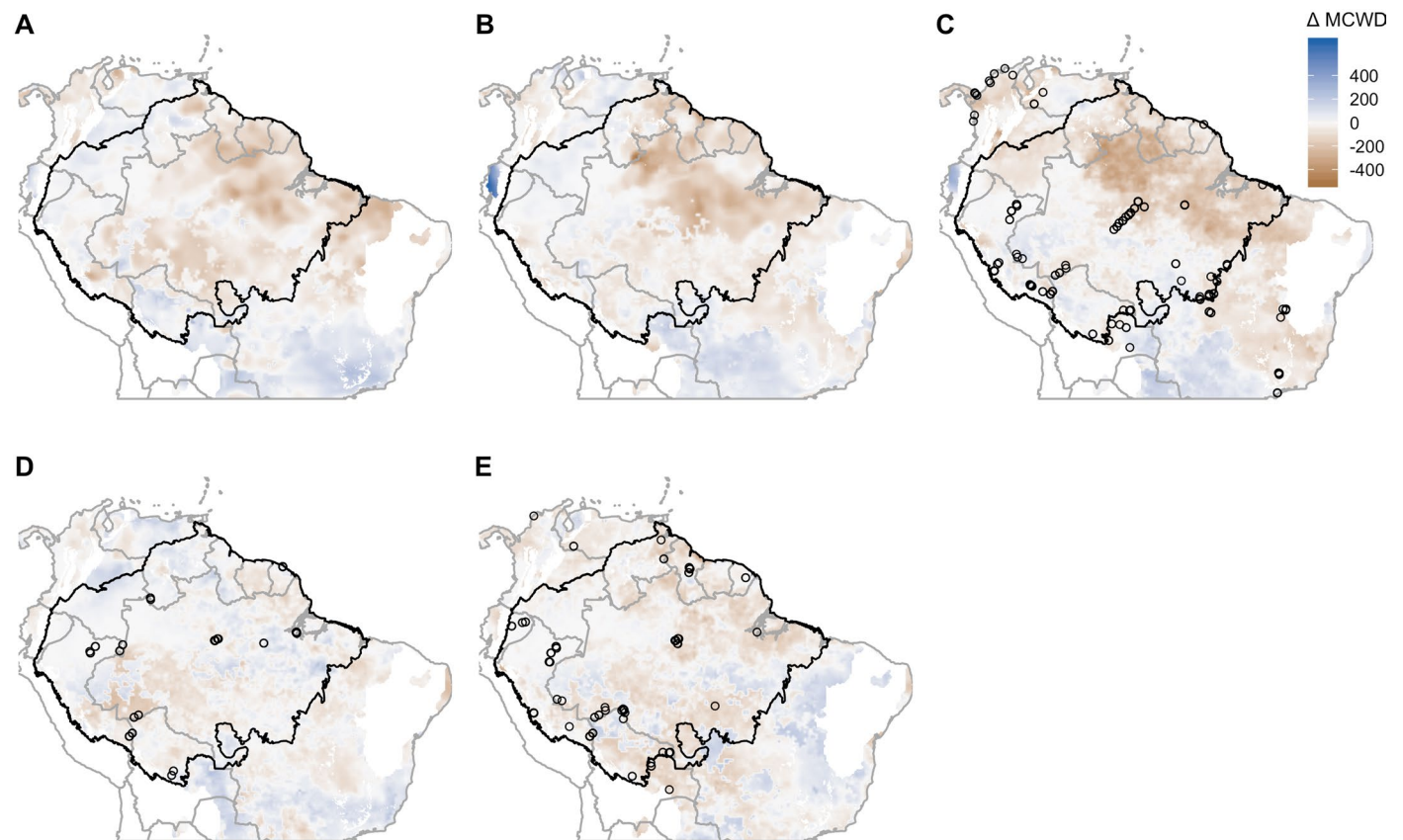
Extended Data Fig. 8 | Standardised effect sizes of change in aboveground biomass carbon in South American tropical forests over the 2015–2016 El Niño, for forests measured after 2000. Points show coefficients from model-averaged linear models, $n = 123$ plots, and error bars show 95% CIs, centred on the mean. Variables that did not occur in well-supported models are shrinkage

adjusted towards zero. Coefficients are standardised so that they represent change in the response variable for one standard deviation change in the explanatory variable. The full models explained 14%, 21% and 7% of variation in Δ net carbon, Δ carbon gains and Δ carbon losses.



Extended Data Fig. 9 | Standardised effect sizes of change in aboveground biomass carbon in South American tropical forests over the 2015–2016 El Niño, as absolute change in carbon. Points show coefficients from model-averaged linear models, $n = 123$, and error bars show 95% CIs, centred on the mean. Variables that did not occur in well-supported models are shrinkage

adjusted towards zero. Coefficients are standardised so that they represent change in the response variable for one standard deviation change in the explanatory variable. The full models explained 11%, 16% and 9% of variation in Δ net carbon, Δ carbon gains and Δ carbon losses.



Extended Data Fig. 10 | Intensity of droughts and locations of forest monitoring plots in South America. Drought anomaly maps for El Niño (top) and non-El Niño (bottom) droughts. El Niño drought anomalies (a–c) are May–April climate years compared to the decade prior, non-El Niño drought anomalies (d, e) are reproduced from (Lopez-Gonzalez et al. 2011 (ref. 53) where October–September years are compared to October 2000–September 2009, excluding

2005. Plot locations are marked as they were analysed in this paper, $n = 123$ (C), and in previous studies; 2005 $n = 55$ (Phillips et al.¹⁰) (D), and 2010 $n = 97$ (Feldpausch et al.¹¹) (E). Core Amazonia is delineated by the black polygon. The shaded area is limited to locations that have $> 1000 \text{ mm yr}^{-1}$ precipitation and are $< 1000 \text{ m}$ above sea level.

Reporting Summary

Nature Research wishes to improve the reproducibility of the work that we publish. This form provides structure for consistency and transparency in reporting. For further information on Nature Research policies, see our [Editorial Policies](#) and the [Editorial Policy Checklist](#).

Statistics

For all statistical analyses, confirm that the following items are present in the figure legend, table legend, main text, or Methods section.

n/a Confirmed

- ☐ ☒ The exact sample size (n) for each experimental group/condition, given as a discrete number and unit of measurement
- ☐ ☒ A statement on whether measurements were taken from distinct samples or whether the same sample was measured repeatedly
- ☐ ☒ The statistical test(s) used AND whether they are one- or two-sided
Only common tests should be described solely by name; describe more complex techniques in the Methods section.
- ☐ ☒ A description of all covariates tested
- ☐ ☒ A description of any assumptions or corrections, such as tests of normality and adjustment for multiple comparisons
- ☐ ☒ A full description of the statistical parameters including central tendency (e.g. means) or other basic estimates (e.g. regression coefficient) AND variation (e.g. standard deviation) or associated estimates of uncertainty (e.g. confidence intervals)
- ☐ ☒ For null hypothesis testing, the test statistic (e.g. F , t , r) with confidence intervals, effect sizes, degrees of freedom and P value noted
Give P values as exact values whenever suitable.
- ☒ ☐ For Bayesian analysis, information on the choice of priors and Markov chain Monte Carlo settings
- ☒ ☐ For hierarchical and complex designs, identification of the appropriate level for tests and full reporting of outcomes
- ☐ ☒ Estimates of effect sizes (e.g. Cohen's d , Pearson's r), indicating how they were calculated

Our web collection on [statistics for biologists](#) contains articles on many of the points above.

Software and code

Policy information about [availability of computer code](#)

Data collection	<p>No software was used for data collection. All field data were uploaded to, and are curated at, ForestPlots.net (ForestPlots.net et al., 2021).</p> <p>References</p> <p>ForestPlots.net et al. Taking the pulse of Earth's tropical forests using networks of highly distributed plots. 260, (2021).</p>
Data analysis	<p>All calculations were performed using the R statistical platform, version 4.0.5 (R Core Team, 2021). We used the R package BiomasaFP, version 0.3.0 (Lopez-Gonzalez, Sullivan & Baker, 2017) to calculate plot aboveground biomass, woody productivity and biomass mortality, including calculating census interval corrections. The R package Rfit, version 0.24.2 (Kloke & McKean, 2012) was used to generate rank-based regression lines, the package MuMIn, version 1.47.5 (Barton, 2019) was used to perform multi-model inference. The lme4 R package, version 1.1.33 (Bates et al., 2022) was used for mixed effects modeling.</p> <p>References</p> <p>R Core Team (2021), R: A language and environment for statistical computing. R Foundation for Statistical Computing, Vienna, Austria. URL https://www.R-project.org/.</p> <p>Lopez-Gonzalez, G., Sullivan, M. J. P. & Baker, T. R. BiomasaFP: Tools for analysing data downloaded from ForestPlots.net. Version 0.3.0 (2015).</p> <p>Kloke, J. D. & McKean, J. W. Rfit: Rank-based estimation for linear models. R Journal, Version 0.24.2. 4, 57–64 (2012).</p> <p>Barton, K. MuMIn: Multi-Model Inference, Version 1.43.17. (2019).</p> <p>Bates, D. et al. lme4: Linear Mixed-Effects Models using 'Eigen' and S4. https://CRAN.R-project.org/package=lme4 (2022).</p>

For manuscripts utilizing custom algorithms or software that are central to the research but not yet described in published literature, software must be made available to editors and reviewers. We strongly encourage code deposition in a community repository (e.g. GitHub). See the Nature Research [guidelines for submitting code & software](#) for further information.

Data

Policy information about [availability of data](#)

All manuscripts must include a [data availability statement](#). This statement should provide the following information, where applicable:

- Accession codes, unique identifiers, or web links for publicly available datasets
- A list of figures that have associated raw data
- A description of any restrictions on data availability

Publicly available climate data used in this paper are available from ERA5 (mean monthly 2-m temperature at 30 km resolution), CRU ts.4.03 (monthly temperature at 0.5° resolution), WorldClim v2 (average temperature and altitude at 1 km²), TRMM product 3B43 V7 (monthly precipitation at 0.25° resolution) and GPCC Version 7 (monthly precipitation at 0.5° resolution).

Source data and R code to generate figures and tables are available from: forestplots.net/publications/datapackages/Bennett-et-al-2023

References

Copernicus Climate Change Service (C3S). ERA5: Fifth generation of ECMWF atmospheric reanalyses of the global climate. Copernicus Climate Change Service Climate Data Store (CDS), accessed 18 Feb 2020 (2017). <https://cds.climate.copernicus.eu/cdsapp#!/dataset/reanalysis-era5-complete?tab=overview>

University of East Anglia Climatic Research Unit, Harris, I. C. & Jones, P. D. CRU TS4.03: Climatic Research Unit (CRU) Time-Series (TS) version 4.03 of high-resolution gridded data of month-by-month variation in climate (Jan. 1901- Dec. 2018). Centre for Environmental Data Analysis, accessed 19 Sep 2019 (2020). https://crudata.uea.ac.uk/cru/data/hrg/cru_ts_4.03/

Fick, S. E. & Hijmans, R. J. WorldClim 2: new 1-km spatial resolution climate surfaces for global land areas. *Int. J. Climatol* 37, 4302–4315 (2017). <http://www.worldclim.com/version2>

Huffman, G. J. et al. The TRMM Multisatellite Precipitation Analysis (TMPA): Quasi-Global, Multiyear, Combined-Sensor Precipitation Estimates at Fine Scales. *Journal of Hydrometeorology* 8, 38–55 (2007). https://disc.gsfc.nasa.gov/datasets/TRMM_3B43_7/summary

Schneider, U. et al. GPCC Full Data Reanalysis Version 6.0 at 0.5°: Monthly Land-Surface Precipitation from Rain-Gauges built on GTS-based and Historic Data: Gridded Monthly Totals. 20-270 MB per decadal gzip compressed NetCDF archive (2011) doi.org/10.5065/D6000072

Field-specific reporting

Please select the one below that is the best fit for your research. If you are not sure, read the appropriate sections before making your selection.

☐ Life sciences ☐ Behavioural & social sciences ☒ Ecological, evolutionary & environmental sciences

For a reference copy of the document with all sections, see nature.com/documents/nr-reporting-summary-flat.pdf

Ecological, evolutionary & environmental sciences study design

All studies must disclose on these points even when the disclosure is negative.

Study description

We worked as a community of more than 100 forest ecologists across South America to produce the first ground-based analysis of the impact of the hottest drought and most extreme El Niño event to date across South American tropical forests. This manuscript presents an assessment of both temperature and drought-responses of intact South American tropical forests. Our multi-decadal, sustained tree-by-tree diameter measurements from 123 long-term forest plots from before, during and after the 2015-2016 climate anomaly provide direct evidence that drier forests are especially vulnerable to drought. Additionally, that the long-term, pre-El Niño biomass carbon sink in South American tropical forests shrank to close to zero during the El Niño.

Research sample

We use data from 123 long-term forest plots in six South American countries.

Sampling strategy

All long-term forest inventory plots analysed are lowland (< 1000 m), closed canopy, mature tropical forests and had been censused at least twice prior to the 2015-16 El Niño event and were censused at least once afterwards. To be included in the analysis plots must also have had no more than five years between the census immediately prior to the El Niño and the census following the El Niño, and these censuses must also have taken place in the same season (within 120 days).

Data collection

Our 123 plots are distributed across 50 distinct clusters in six countries: Bolivia, Brazil, Colombia, French Guiana, Peru and Venezuela. All permanent inventory plots are part of the RAINFOR or PPBIO forest plot networks. See Table S1 for plot details. In each plot all trees ≥100 mm diameter are measured, tagged with a unique identifier, and identified to species, where possible. Tree diameter was measured at 1.3 m along the stem from the ground, or above buttresses, if present, using standardised methods for all plots (Phillips et al., 2010). In some cases, the point of diameter measurement (POM) had to be moved due to upward growth of buttresses or deformities. For these trees we calculated a single common estimate of growth before and after the POM-change. Stems that reached a diameter ≥100 mm during the census interval were recorded as new recruits. We estimated tree aboveground mass using the allometric equation: $AGB = 0.0673 \times (\rho D^2 H)^{0.97637}$, where ρ is stem wood density (g cm⁻³), D is stem diameter (cm) at 1.3 m or above buttresses, and H is height (m). We estimate the aboveground mass of palms using the equation in Goodman et al. (2013). Wood density measurements were compiled mostly from the Global Wood Density Database on the Dryad digital repository (datadryad.org) (Chave et al., 2009, Zanne et al., 2009) and each individual stem in a plot was matched to a species-specific mean wood density value, where possible. For incompletely identified individuals or individuals belonging to species not in the wood density database, we use the mean wood density value for genus if available, then family. For unidentified individuals, we used the mean wood density value of all individual trees in the plot (Lopez-Gonzalez et al., Lewis et al., 2009).

To estimate height for plots or trees a 3-parameter regional height-diameter Weibull equation was fitted using the local.heights function in the BiomasaFP R package (Lopez-Gonzalez et al., 2015). We estimated the aboveground biomass in live stems, aboveground wood productivity, and AGB mortality, in Mg dry mass ha⁻¹, at each census of each plot, and corrected for census-interval effects (Talbot et al., 2014).

References

ForestPlots.net et al. Taking the pulse of Earth's tropical forests using networks of highly distributed plots. 260, (2021).
 Phillips, O.L. et al. RAINFOR field manual for plot establishment and remeasurement. (2010)
 Brien, R. J. W. et al. Long-term decline of the Amazon carbon sink. Nature 519, 344–348 (2015).
 Hubau, W. et al. Asynchronous carbon sink saturation in African and Amazonian tropical forests. Nature 579, 80–87 (2020).
 Qie, L. et al. Long-term carbon sink in Borneo's forests halted by drought and vulnerable to edge effects. Nature Communications 8, 1966 (2017).
 Lewis, S. L. et al. Above-ground biomass and structure of 260 African tropical forests. Philosophical Transactions of the Royal Society B: Biological Sciences 368, 20120295–20120295 (2013).
 Chave, J. et al. Towards a worldwide wood economics spectrum. Ecology Letters 12, 351–366 (2009).
 39. Zanne, A. E. et al. Data from: Towards a worldwide wood economics spectrum. Dryad Digital Repository. (2009) doi:10.5061/dryad.234.
 Lopez-Gonzalez, G., Lewis, S. L., Burkitt, M. & Phillips, O. L. ForestPlots.net: a web application and research tool to manage and analyse tropical forest plot data. Journal of Vegetation Science 22, 610–613 (2011).
 Lewis, S. L. et al. Increasing carbon storage in intact African tropical forests. Nature 457, 1003–1006 (2009).
 Sullivan, M. J. P. et al. Field methods for sampling tree height for tropical forest biomass estimation. Methods in Ecology and Evolution 9, 1179–1189 (2018)
 Lopez-Gonzalez, G., Sullivan, M. J. P. & Baker, T. R. BiomasaFP: Tools for analysing data downloaded from ForestPlots.net. Version 0.3.0 (2015).
 Talbot, J. et al. Methods to estimate aboveground wood productivity from long-term forest inventory plots. Forest Ecology and Management 320, 30–38 (2014).

Timing and spatial scale	The 123 plots have a median plot size of 1 ha, mean 1.05 ha (range 0.25 - 6.25 ha), with a total plot area of 128.7 ha. While some plots were established as early as 1962, to support temporal consistency among plots, and to avoid potential impacts of the 1982–1983 El Niño event, we include only censuses after 1983. Any additional censuses after the El Niño census were not used in this analysis. Plots were measured at least three times and a maximum of 27 times between 1984 and 2018. The plot monitoring periods span 3 to 32 years; mean initial census was May 2001, mean pre-El Niño census was September 2014, and mean post-El Niño census was May 2017. The mean pre-El Niño monitoring length was 13.3 years and the mean length of the El Niño interval was 2.7 years. See Table S1 for plot census details.
Data exclusions	Plots were selected using the criteria described above (see Sampling strategy section). Plots that did not meet one or several of these criteria were not used for analysis.
Reproducibility	Our analysis did not include experimental findings. All source data and code to rerun analysis and reproduce figures can be found at forestplots.net/data-packages/Bennett-et-al-2023.
Randomization	No randomization occurred in our study.
Blinding	Blinding was not relevant to our study.
Did the study involve field work?	<input checked="" type="checkbox"/> Yes <input type="checkbox"/> No

Field work, collection and transport

Field conditions	All 123 plots are located in lowland (<1000 m), closed canopy, mature, South American tropical forests. The El Niño remeasurement campaigns took place between April 2016 and October 2018.
Location	Plots are located between -23.4oS to 11.2oN latitude and 77.5oW to 44.2oW. A map showing locations of all plots is presented in Figure 1, and plot latitude and longitude is in Table S1.
Access & import/export	Plot inventory El Niño remeasurement census data were collected by teams led by at least one of the researchers co-authoring this paper. This paper is a product of the RAINFOR and PPBio networks. These permanent inventory plot networks only exist because of huge community effort. A full list of people involved in data collection can be found in the Acknowledgments.
Disturbance	No significant disturbance was caused by our measurements. Stems were tagged using a single aluminium nail (no iron), avoiding damage to trees due to corrosion.

Reporting for specific materials, systems and methods

We require information from authors about some types of materials, experimental systems and methods used in many studies. Here, indicate whether each material, system or method listed is relevant to your study. If you are not sure if a list item applies to your research, read the appropriate section before selecting a response.

Materials & experimental systems

- | | |
|-------------------------------------|--|
| n/a | Involved in the study |
| <input checked="" type="checkbox"/> | <input type="checkbox"/> Antibodies |
| <input checked="" type="checkbox"/> | <input type="checkbox"/> Eukaryotic cell lines |
| <input checked="" type="checkbox"/> | <input type="checkbox"/> Palaeontology and archaeology |
| <input checked="" type="checkbox"/> | <input type="checkbox"/> Animals and other organisms |
| <input checked="" type="checkbox"/> | <input type="checkbox"/> Human research participants |
| <input checked="" type="checkbox"/> | <input type="checkbox"/> Clinical data |
| <input checked="" type="checkbox"/> | <input type="checkbox"/> Dual use research of concern |

Methods

- | | |
|-------------------------------------|---|
| n/a | Involved in the study |
| <input checked="" type="checkbox"/> | <input type="checkbox"/> ChIP-seq |
| <input checked="" type="checkbox"/> | <input type="checkbox"/> Flow cytometry |
| <input checked="" type="checkbox"/> | <input type="checkbox"/> MRI-based neuroimaging |